Possible many-body localized phases in Aubry-André systems

by

Sara Sharifan

A Thesis submitted to the Faculty of Graduate Studies of
The University of Manitoba
in partial fulfillment of the requirements of the degree of

MASTER OF SCIENCE

Department of Physics and Astronomy
University of Manitoba
Winnipeg

Abstract

Anderson localization, where quenched disorder leads to the localization of single-particle wave functions, has been studied extensively. However, the effect of interaction and non-random potentials on many-body localization (MBL) has gained attention recently. We investigate the dynamics of the interacting Aubry-André model to assess the stability of the many-body localized (MBL) phase. Our motivation to consider the Aubry–André potential as the disorder potential is to eliminate the avalanche mechanism, which often destabilizes MBL in systems with quenched disorder. We analyze the time evolution and the system-size scaling across a range of disorder strengths for the entanglement entropy, number entropy, and the Hartley number entropy. In the non-interacting case, our results confirm an Anderson localization transition at a critical disorder strength $D_c = 2$, which is consistent with earlier studies. However, when interactions are introduced, the number entropy appears to grow unboundedly as $S_N \sim \ln \ln t$ in the thermodynamic limit, even for large disorder. Meanwhile, the entanglement entropy grows logarithmically, $S \sim \ln t$, and both entropies saturate in a correlated manner at finite times $t_d \sim e^{LD}$. These findings suggest that using a quasiperiodic potential to remove the avalanche mechanism does not stabilize true MBL behavior. Instead, the long-time dynamics are qualitatively similar to those found in systems with random disorder. In this thesis, we first introduce the fundamental concepts of thermalization, quantum quench, and symmetry-resolved entropies, then provide a study of localization, specifically in the Aubry-André model. Finally, we place our numerical results in the broader context of the current debate on the stability of many-body localized phases.

Acknowledgements

I would like to express my deepest appreciation to my supervisor, Dr. Jesko Sirker, for his continuous guidance and support from the very beginning of my master's program. His profound expertise in the field was critical in developing this thesis. I am especially grateful to him for not only guiding me intellectually and providing me with feedback, but also for being considerate and mindful of my personal well-being during times of homesickness and anxiety. Therefore, I am looking forward to pursuing my Ph.D. with him as a supervisor again. I would like to extend my sincere thanks to Dr. Maximilian Kiefer-Emmanouilidis for generously sharing his knowledge in the field and helping me in executing GPU-based simulations, insights that significantly benefited this work. I am also thankful to Dr. Kyle Monkman for his helpful advice and occasional help with my research questions. This research relied on computational resources provided by the Grex high-performance computing cluster at the University of Manitoba and by clusters such as Béluga through the Digital Research Alliance of Canada, to which access was kindly provided by Dr. Sirker. I also wish to recognize the support provided by the Department of Physics and Astronomy at the University of Manitoba through a graduate stipend, and I wish to thank Susan Beshta, graduate program advisor, for her assistance throughout my program. On a personal note, I am extremely fortunate for the emotional support of my parents and brother throughout my time in Canada. Their belief in me carried me through this journey. I also wish to thank my uncle, whose enduring confidence in me has been a source of motivation throughout my academic path.

Contents

List of Figures

Chapter 1

Introduction

In quantum statistical mechanics, one important question we are interested in is understanding how and when subsystems of an isolated quantum many-body system reach thermal equilibrium. Closed systems that are initialized far from equilibrium are generally expected to undergo thermalization in the sense that their subsystems will behave as if they are in contact with a thermal bath, while the closed system as a whole will remain in a pure state. Statistical mechanics then emerges from unitary quantum evolution and a subsequent partial trace, and the memory of the initial state is lost. However, not all quantum systems follow this expectation. Integrable systems are one of these exceptions, and they fail to fully erase the memory of initial states. Another exception is the phenomenon of localization that we are interested in. Localization, where quantum transport stops and the system avoids thermalizing, was first introduced in 1958 by Anderson [1], who demonstrated that interference effects in disordered systems can prevent single-particle wavefunctions from spreading across the system. This is known as Anderson localization (AL) and results in the complete suppression of transport, formation of spatially localized eigenstates, and the absence of diffusion in non-interacting systems. It was believed that introducing interactions to the system would restore ergodicity by dephasing and thermal fluctuations. Then, in 2006, Basko, Aleiner, and Altshuler argued otherwise [2]. They expressed that many-body eigenstates could remain localized even in the presence of interactions. This gave rise to the concept of many-body localization (MBL), representing a breakdown of thermalization in interacting systems.

In the MBL phase after a quantum quench, a sudden change in the Hamiltonian of

the system, the system follows unitary time evolution, and unlike ergodic systems, it retains the memory of the initial state and exhibits logarithmic entanglement growth, $S(t) \sim \ln t$, rather than the linear growth of thermalizing phases. In the system with conserved number of particles, number entropy, which captures the growth of particle-number fluctuations between subsystems, is another observable and in the localized phase it is expected to saturate quickly as the particles are confined to local regions. However, recent numerical studies by Kiefer-Emmanouilidis and Sirker et al. [3], demonstrated otherwise. Their findings show that number entropy continues to grow slowly in time, following a double-logarithmic scaling $S_N \sim \ln \ln t$, and questioning the stability of MBL in line with concerns previously expressed by Suntajs et al. [4] in 2019. This existing growth raises the question whether there is a specific type of potential disorder for which the MBL phase truly supports fully frozen particle transport. In systems with random potentials, rare regions where the potential varies slowly can form locally ergodic subsystems. These regions can eventually thermalize their surroundings in a process known as the avalanche mechanism and destabilize the MBL phase in the thermodynamic limit [5].

Quasiperiodic disorders have gained attention in recent studies since these models prevent producing rare region fluctuations and avalanche mechanisms. The Aubry-André (AA) potential has been used as a quasiperiodic disorder in experiments to observe MBL in interacting ultracold atomic systems [6], and has been claimed to show more stability of MBL compared to the random potential case in numerical studies [7]. Our findings show that while in the absence of interaction, the AA model experiences Anderson localization with a sharp transition at a critical disorder, a system with interaction shows correlated von Neumann and number entropies behavior, consistent with previous results in random systems. Even by our choice of the model and the absence of avalanches, we observed that the number and Hartley number entropies grow slowly in time. This indicates that the many-body system, even in a quasiperiodic potential, seems to not exhibit true localization. The scaling behaviors we extract closely match previous studies, suggesting that quasiperiodicity does not fundamentally change the long-time dynamics. This thesis is organized as follows: In Ch. 2, we focus on thermalization in quantum systems and introduce essential concepts such as quantum quenches and symmetry-resolved entropies, which are the basis for analyzing non-equilibrium dynamics. In Ch. 3, we explore the transition from diffusion to localization, starting with Anderson localization and scaling theory, then

introducing many-body localization with various diagnostic tools, including entanglement entropy and number entropy. Ch. 4 introduces the model and methodology used in this study and discusses numerical techniques such as exact diagonalization and Trotter-Suzuki decomposition. In Ch. 5 we present our main results, including the time evolution of different entropies under different disorder strengths, and contrasts between interacting and non-interacting systems. Finally, Ch. 6 summarizes our findings and discusses their implications in the ongoing debate about the stability of the MBL phase in the thermodynamic limit.

Chapter 2

Thermalization in Quantum Systems

Thermalization is a fundamental concept in the research of many-body quantum dynamics. One of the main open questions is: How do isolated quantum systems develop toward thermal equilibrium? [8] Or in other words, how does a closed quantum system reach a state where the expectation values of local observables resemble those of a thermal ensemble? While for classical systems, thermalization is very well understood within the statistical mechanics framework, marked by a uniform temperature and other macroscopic features achieved through ergodicity, it remains an interesting challenge for quantum systems due to the interplay between the unitary nature of their time evolution and the entanglement [9, 10, 11]. A quantum system in thermal equilibrium is fully specified by a few parameters, such as temperature and chemical potential, each of which corresponds to an extensive conserved quantity [12]. This would imply that thermalization is accompanied by losing the system's memory about its initial state. However, unitary time evolution cannot erase this information, and in a closed system, all quantum information about the initial state is always preserved [8]. In these quantum systems, the existence of entanglement in quantum states makes the thermalization process different. Spreading quantum entanglement renders information about the initial state locally inaccessible and requires global measurements [13].

Quantum thermalization finds its grounds in the quantum ergodic theorem by von Neumann which states that a generic quantum system explores all its accessible states

within the same energy shell uniformly in time [14]. This theorem connects quantum mechanics and statistical mechanics by explaining how quantum systems approach thermal equilibrium. It points out the connection between time averages and ensemble averages. The long-time average of an observable in an ergodic closed quantum system mirrors its value predicted by a microcanonical ensemble. This insight provides a statistical interpretation of quantum dynamics and explains how thermal equilibrium emerges without requiring external reservoirs. Since von Neumann's foundational work, the field has been considerably influenced by developments in quantum chaos, which is beyond the scope of this thesis.

The formulation of the Eigenstate Thermalization Hypothesis (ETH) is arguably one of the significant advances in understanding quantum thermalization [9, 8]. However, ETH is not applicable to all systems and its validity remains an open question. Alternative methodologies for comprehending thermalization do not depend on ETH and focus on the role of conserved quantities and subsystem interactions in determining thermal behavior. These methods emphasize the significance of locality and conserved charges in ascertaining thermal behavior [15, 16]. Comprehending thermalization in quantum systems holds potential applications in the advancement of quantum memory and quantum information processing, particularly for the preservation of information over extended durations [8]. This section examines the mechanism of quantum thermalization, quantum quench, and the criteria that determine whether quantum systems may thermalize.

2.1 Fundamentals of Quantum Thermalization

To begin, it is necessary to distinguish between two types of quantum states, known as *pure* and *mixed*. Pure states, described by wavefunctions $|\psi\rangle$, a vector in a Hilbert space $\mathcal{H}$, capture the complete quantum mechanical description of a system at a given time. These states are critical for characterizing isolated quantum systems where interactions with an external environment are absent. Unlike pure states, mixed states, described by density matrices ρ, include the possibility of a statistical mixture of quantum states due to the uncertainty in the state of the system induced by interactions with the environment. Mixed states often represent systems in thermal equilibrium, known as a thermal ensemble [9]. In this state, the subsystem attains

maximum of entropy. The density matrix for a mixed state is represented as

$$\rho = \sum_i p_i |\psi_i\rangle\langle\psi_i|,$$

where p_i denotes the probability linked to the pure states $|\psi_i\rangle$, according to the stipulated requirements $\sum_i p_i = 1$. It is important to recognize that a density matrix can be defined even for a system in a pure state

$$\rho = |\psi\rangle\langle\psi|.$$

This is especially pertinent when examining subsystems of a larger isolated system. In contrast to the real world, quantum mechanics often assumes that systems are closed or isolated, lacking interaction with an external environment. Consequently, the overall state of the system remains pure throughout its temporal evolution [9]. We might once again inquire: how does an isolated quantum system achieve thermalization while its overall state remains pure? The state of a subsystem typically seems mixed because of its entanglement with the remainder of the system [8]. The subsystem's mixed state can attain thermal equilibrium, resulting in its thermalization [10]. The process of thermalization in a quantum system fundamentally represents the redistribution of quantum correlations among various components of the system, resulting in memory loss within local observables in subsystems and eventually a state of equilibrium [11]. This arises from quantum entanglement[17].

The density matrix formalism offers a concise method for computing expectation values of quantum observables [18]. The expectation value of an observable $\hat{O}$ in the state described by the density matrix ρ is expressed as

$$\langle\hat{O}\rangle = \mathrm{Tr}(\rho\hat{O}), \tag{2.1}$$

where Tr signifies the trace, or the summation of the diagonal elements in the resultant matrix. This approach emphasizes the significance of density matrices in representing statistical mixtures, especially in isolated systems, where pure states inadequately reflect thermodynamic behavior [18].

In the case of an isolated quantum system, where the external potential is constant, we introduce the Hamiltonian, $\hat{H}$, a Hermitian operator that represents the total

energy of the system [10] and the Schrödinger equation that delineates how a quantum state changes over time [11]

$$i\hbar\frac{d}{dt}|\psi(t)\rangle = \hat{H}|\psi(t)\rangle. \tag{2.2}$$

Here, $\hbar$ denotes the reduced Planck constant, and $|\psi(t)\rangle$ represents the quantum state at time t. This equation describes how the state evolves in time due to the Hamiltonian $\hat{H}$. The unitary evolution of states implies the conservation of energy if $\hat{H}$ is time independent [9]. The concept of unitary time evolution requires a unitary transformation that the evolution of a quantum system in time is governed by. Mathematically, given a quantum state $|\psi(t)\rangle$, its time evolution is given by

$$|\psi(t)\rangle = \hat{U}(t, t_0)|\psi(t_0)\rangle, \tag{2.3}$$

where $\hat{U}(t, t_0)$ is the time evolution operator. The unitary nature of this operator ensures the conservation of probability. Unitary evolution preserves all initial information which presents a contradiction with what we mentioned earlier: thermal equilibrium in a quantum system suggests that the system has lost memory of its initial state. However, the paradox is resolved through decoherence which means that the initial state's local properties are not erased but become hidden within the system's entanglement structure. As entanglement spreads, retrieving the initial information requires measuring global operators, making it practically inaccessible [13]. This process results in the thermal behavior in subsystems while the overall system's information has remained the same.

We consider our closed system partitioned into two, a subsystem A and its environment B. As the system thermalizes, subsystem A appears to be in thermal equilibrium with the rest of the system acting as a reservoir. To examine the local observables and entanglement within the subsystem, calculating the reduced form of the density matrix can be beneficial. The Hilbert space of this combined system, $\mathcal{H}$, can be obtained by the tensor product of the Hilbert spaces of A and B, $\mathcal{H} = \mathcal{H}_A \otimes \mathcal{H}_B$. An arbitrary state of this system, $|\psi\rangle \in \mathcal{H}$, can be expressed as a superposition of basis states from $\mathcal{H}_A$ and $\mathcal{H}_B$

$$|\psi\rangle = \sum_{i,j} c_{ij}|i\rangle_A|j\rangle_B, \tag{2.4}$$

where $|i\rangle_A$ and $|j\rangle_B$ are basis states of subsystems A and B, respectively, and c_{ij} are complex coefficients. To obtain the reduced density matrix of subsystem A, ρ_A, one must trace out the degrees of freedom of subsystem B from the density matrix of the complete system ρ,

$$\rho_A = \mathrm{Tr}_B(\rho), \tag{2.5}$$

where Tr_B represents the partial trace over subsystem B. $\rho = |\psi\rangle\langle\psi|$ is the density matrix of the whole system. Then

$$\rho_A = \mathrm{Tr}_B(|\Psi\rangle\langle\Psi|) = \sum_{i,j,k} c_{ik}c_{jk}^*|i\rangle_A\langle j|_A. \tag{2.6}$$

Additionally, an observable $\hat{O}_A$ in subsystem A is represented by a Hermitian operator acting on $\mathcal{H}_A$ and the expectation value of $\hat{O}_A$ in the state $|\psi\rangle$ can be calculated using ρ_A as follows

$$\langle\hat{O}_A\rangle = \mathrm{Tr}(\hat{O}_A\rho) = \mathrm{Tr}_A(\hat{O}_A\rho_A), \tag{2.7}$$

where Tr_A denotes the trace over subsystem A.

In quantum systems, the von Neumann entropy, defined as $S(\rho) = -Tr(\rho\log\rho)$, serves as a measure of entanglement when applied to the reduced density matrix of a subsystem. For a system in a pure state $\rho = |\Psi\rangle\langle\Psi|$, $S(\rho) = 0$, but for a subsystem, it quantifies the non-local correlation between the subsystem and the rest of the system [19]. Here, the reduced density matrix is key to understanding entanglement phenomena [20]. The von Neumann entropy of subsystem A, $S(\rho_A) = -\mathrm{Tr}(\rho_A\log\rho_A)$, measures the entanglement between subsystems A and B, and $S(\rho_A)$ is maximal when the state is maximally entangled [21]. This concept is very crucial to our research topic and will be fully reviewed in the next chapter. Another aspect of quantum systems that needs attention is the existence of conservation laws. Conservation laws, including energy conservation and particle number conservation, restrict the dynamics of the system and determine whether the system thermalizes or not [10]. Energy conservation arises from the time independence of the Hamiltonian. Thus, in the context of closed quantum systems, this implies that the expectation value of the Hamiltonian remains the same over time.

$$\frac{d}{dt}\langle \hat{H} \rangle = 0. \tag{2.8}$$

We also often have a conservation of the particle number in many quantum systems. The particle number operator $\hat{N}$ then commutes with the Hamiltonian, i.e., $[\hat{H}, \hat{N}] = 0$, expressing that the particle number is conserved [10].

2.2 Quantum Quench

Quantum quench refers to a sudden change in the Hamiltonian of a system, often achieved by abruptly changing some parameters of the system, such as interaction strength or an external potential [10]. This sudden change initiates a complex process of relaxation and thermalization. There are two typical scenarios of quench dynamics: global quenches and local quenches. The simplest form of a quantum quench is a global quench, where the change in the Hamiltonian parameters is uniform throughout the system. This can be achieved, for example, by abruptly changing the strength of an external field that couples to all the degrees of freedom in the system. In this scenario, the system initially prepared in an eigenstate of the initial Hamiltonian H_0 is suddenly subjected to a new Hamiltonian $\hat{H}$ at time $t = 0$ by suddenly changing a control parameter λ in the Hamiltonian to λ' [10].

$$H(t) = \begin{cases} H_0 & \text{for } t < 0 \\ H & \text{for } t \geq 0 \end{cases} \tag{2.9}$$

Following a quantum quench, a system typically undergoes unitary time evolution under the final Hamiltonian H and the state of the system at a later time t can be described by the time-evolved wavefunction

$$|\Psi(t)\rangle = e^{-iHt}|\Psi(0)\rangle = \sum_n e^{-iE_n t}|n\rangle\langle n|\Psi(0)\rangle. \tag{2.10}$$

Here, $|n\rangle$ and E_n are the eigenstates and eigenenergies of $\hat{H}$, respectively. If the state $|\Psi(0)\rangle$ is not an eigenstate of $\hat{H}$, a complicated dynamics ensues, which investigates the dynamics of quantum many-body systems far from equilibrium. However, for many-particle systems, one often focuses on the time evolution of specific, typically

local, observables, since the full quantum state $|\Psi(t)\rangle$ is difficult to compute and measurements are usually local.

$$\langle \hat{O}(t) \rangle = \langle \Psi(t) | \hat{O} | \Psi(t) \rangle = \sum_{n,m} e^{-i(E_n - E_m)t} \langle m | \Psi(0) \rangle \langle \Psi(0) | n \rangle \langle n | \hat{O} | m \rangle \tag{2.11}$$

The importance of quantum quenches lies in their ability to investigate the dynamics of observables, entanglement growth, and energy redistribution in the Hilbert space. After a global quantum quench, energy is conserved for all $t > 0$. However, the energy density after a quench is in general larger than the ground-state energy density of the system, E_0 [10].

$$e = \lim_{L \to \infty} \frac{1}{L} \langle \Psi(t) | \hat{H} | \Psi(t) \rangle > \lim_{L \to \infty} \frac{E_0}{L}. \tag{2.12}$$

This indicates the larger exploration of Hilbert space following a quench. One of the following scenarios can occur:

Thermalization: The subsystem of the quantum system eventually reaches a steady state described by a thermal Gibbs ensemble, which is characterized by a temperature and other thermodynamic quantities. In this case, local observables relax to their thermal equilibrium values.

Non-thermalization: In some cases, the system does not thermalize, but rather relaxes to a stationary state that retains memory of the initial conditions. In integrable systems, this case happens due to the presence of many conserved quantities. These restrict the system's dynamics, and lead to a steady state described by a Generalized Gibbs Ensemble (GGE). In another type of systems, ones with strong disorder, many-body localization (MBL), if it exists, could prevent the spread of energy and entanglement, thus preventing a system from being ergodic and from thermalizing.

As mentioned numerous times above, the presence of conserved quantities determines whether a system thermalizes. These laws apply constraints on the system's dynamics and govern the distribution of energy and other conserved quantities. Systems with a small number of conserved quantities, such as energy, often thermalize because information about the initial state becomes effectively hidden in the many

degrees of freedom [8, 9]. In many-body systems, two broad categories of conservation laws can be identified: local and non-local conserved quantities. Local conserved quantities, including energy and particle number, are associated with symmetries that act within finite regions of the system and dictate the system's relaxation properties. For a closed quantum system, energy is always a conserved quantity. The energy expectation value can be expressed as

$$\langle \hat{H} \rangle = \mathrm{Tr}(\rho(t)\hat{H}) = \mathrm{Tr}\left(e^{-i\hat{H}t}\rho(0)e^{i\hat{H}t}\hat{H}\right) = \mathrm{Tr}(\rho(0)\hat{H}). \tag{2.13}$$

This relation reflects that the energy of the system is encoded in the density matrix. On the other hand, as mentioned before, in an isolated quantum system, subsystems can act as baths for each other, causing thermalization. This system, with no other conserved quantities, is expected to locally relax to thermal equilibrium. This mechanism of internal thermalization is relevant to the thermodynamic limit, where the size of B is much larger than A. The reduced density matrix of A then becomes locally equivalent to a thermal Gibbs state,

$$\rho_A \approx \rho_{A,\mathrm{Gibbs}} \approx \frac{e^{-\beta\hat{H}_A}}{\mathrm{Tr}(e^{-\beta\hat{H}_A})}, \tag{2.14}$$

where $\hat{H}_A$ is the Hamiltonian of subsystem A, and β is the inverse temperature fixed by the energy density e of the initial state $\hat{\rho}(0)$ of the whole system

$$e \equiv \lim_{L\to\infty} \frac{1}{L}\mathrm{Tr}(\hat{\rho}(0)\hat{H}) = \lim_{L\to\infty} \frac{1}{L}\mathrm{Tr}(\hat{\rho}_{\mathrm{Gibbs}}\hat{H}). \tag{2.15}$$

While β is calculated from the global energy density, it governs subsystem A to thermalize through Eq. (2.14).

Systems with many conserved quantities or local integrals of motion, such as integrable systems, fail to thermalize and instead reach a non-thermal steady state [12]. These conserved quantities act globally across the entire system and significantly constrain the dynamics, preventing complete thermalization. Instead of a thermal Gibbs ensemble, integrable systems relax to a generalized Gibbs ensemble (GGE), characterized by the extensive set of conserved quantities $\hat{\eta}_n$ which $[\hat{H}, \hat{\eta}_n] = 0$ [8].

The GGE is described by the density matrix

$$\rho_{\mathrm{GGE}} = \frac{e^{-\sum_n \lambda_n \hat{\eta}_n}}{\mathrm{Tr}(e^{-\sum_n \lambda_n \hat{\eta}_n})},$$

where $\hat{\eta}_n$ are the conserved quantities, and λ_n are Lagrange multipliers determined by the initial conditions. These are fixed by ensuring that

$$\langle \psi(0)|\hat{\eta}_n|\psi(0)\rangle = \mathrm{Tr}(\rho_{\mathrm{GGE}}\hat{\eta}_n). \tag{2.16}$$

2.2.1 Symmetry-Resolved Entropies

Investigating various quantum phases and transitions in quantum systems requires the measurement of entanglement, as it provides information about correlations within the system. Entropy quantifies the information contained within quantum states and correlations between subsystems. Thus, entanglement measurement is by its very nature associated with entropy including von Neumann entropy and Rényi entropies. These entropies provide beneficial scaling characteristics to distinguish phases of matter and investigate dynamics within many-body systems [10, 22, 17].

Entropy is naturally linked to the formalism of the density matrix in quantum mechanics. The von Neumann entropy of a subsystem A, which measures the entanglement between A and the rest of the system, is defined as [14]

$$S_A = -\mathrm{Tr}(\rho_A \log \rho_A), \tag{2.17}$$

where $\rho_A = \mathrm{Tr}_B(\rho)$ and B is the complement of A in the whole system. In an isolated system that undergoes a unitary time evolution, the von Neumann entropy of the entire system remains constant [23]. However, the local entropy, defined for a subsystem, can increase [9]. Higher von Neumann entropy of the reduced density matrix leads to a larger degree of entanglement, loss of accessible information about the initial conditions, and more disorder in the subsystem. In other words, the higher the entropy, the lower our knowledge about the state of the system is.

In a system with a conserved number of particles, the von Neumann entropy can be broken down into two distinct terms, *number entropy* and *configurational entropy*

$$S = S_N + S_C. \tag{2.18}$$

This decomposition follows from the conservation of particle number in the system. The total number operator $\hat{N}$ commutes with the Hamiltonian, $[\hat{N}, \hat{H}] = 0$, which implies $[\hat{N}, \rho] = 0$. Consequently, the particle number operator in subsystem A, $\hat{N}_A$, also commutes with the reduced density matrix, $[\hat{N}_A, \rho_A] = 0$. In the particle number basis one has $\hat{N}_A|n, \alpha\rangle = n|n, \alpha\rangle$, and thus

$$\langle n, \alpha|[\hat{N}_A, \rho_A]|m, \beta\rangle = 0 \qquad (n \neq m). \tag{2.19}$$

This implies that ρ_A is block diagonal in this basis,

$$\rho_A = \begin{pmatrix} \rho_0 & 0 & 0 & \cdots \\ 0 & \rho_1 & 0 & \cdots \\ 0 & 0 & \rho_2 & \cdots \\ \vdots & \vdots & \vdots & \ddots \end{pmatrix}. \tag{2.20}$$

The reduced density matrix can be written using the projector $\hat{P}_{N_A}$ onto the subspace with N_A particles in A as

$$\rho_A = \sum_{N_A} \hat{P}_{N_A} \rho_A \hat{P}_{N_A} = \sum_{N_A} \rho_{N_A}, \tag{2.21}$$

where $\rho_{N_A} = \hat{P}_{N_A} \rho_A \hat{P}_{N_A}$, and the probability of finding N_A particles in A is $\mathrm{Tr}(\rho_{N_A}) = p_A(N_A)$. Introducing the normalized block density matrices

$$\rho_A^{(N_A)} = \frac{\rho_{N_A}}{p_A(N_A)}, \qquad \mathrm{Tr}(\rho_A^{(N_A)}) = 1, \tag{2.22}$$

the reduced density matrix takes the form

$$\rho_A = \sum_{N_A} p_A(N_A) \rho_A^{(N_A)}. \tag{2.23}$$

Substituting Eq. (2.23) into the von Neumann entropy of Eq. (2.17), one finds

$$S_A = -\sum_{N_A} \mathrm{Tr}\Big(p_A(N_A) \rho_A^{(N_A)} \ln \Big[p_A(N_A) \rho_A^{(N_A)} \Big] \Big). \tag{2.24}$$

This expands to

$$S_A = -\sum_{N_A} p_A(N_A) \ln p_A(N_A) - \sum_{N_A} p_A(N_A) \mathrm{Tr}\left(\rho_A^{(N_A)} \ln \rho_A^{(N_A)}\right). \tag{2.25}$$

The first term,

$$S_N = -\sum_{N_A} p_A(N_A) \ln p_A(N_A), \tag{2.26}$$

represents the *number entropy*, which captures the uncertainty in the particle number distribution in subsystem A. The second term,

$$S_C = \sum_{N_A} p_A(N_A) S(\rho_A^{(N_A)}), \text{ with } S(\rho_A^{(N_A)}) = -\mathrm{Tr}\left(\rho_A^{(N_A)} \ln \rho_A^{(N_A)}\right), \tag{2.27}$$

is the *configurational entropy*, which quantifies the entanglement within each particle number sector. This decomposition can address the difficulties faced in measuring the entanglement entropy in experiments despite advancements in areas such as cold atomic gases and trapped-ion systems [24, 25, 26, 13, 27]. Number entropy is particularly useful because it depends entirely on the particle distribution within the system and therefore provides a direct probe of transport properties and how particles spread through the system. It has been effectively used in theoretical studies of phases of matter [28].

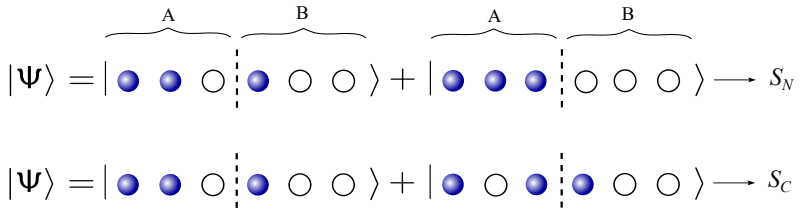

Figure 2.1: Schematic representation of subsystem bipartitioning into regions A and B, illustrating contributions to number entropy, S_N, from particle number fluctuations and to configurational entropy, S_C, from distinct particle arrangements within the same number sector.

Although the von Neumann entropy has been successfully used in studies on many-body localization, a new set of entropies, *Rényi entropies*, has gained significant attention in recent studies. The Rényi entropies provide entanglement measurements

that generalize the von Neumann entropy. The Rényi entropy of order α is defined as

$$S^{(\alpha)} = \frac{1}{1-\alpha} \ln \left(\mathrm{Tr}(\rho_A^\alpha) \right), \tag{2.28}$$

where $\alpha > 0$ and $\alpha \neq 1$. In the limit $\alpha \to 1$, the Rényi entropy reduces to the von Neumann entropy. Different values of α refer to different features of quantum states, such as the *Hartley entropy* ($\alpha \to 0$) and the *second Rényi entropy* ($\alpha = 2$). Decomposition of Rényi entropy into the number Rényi entropy and configurational Rényi entropy is possible in the presence of a globally conserved particle number. We can define the Rényi number entropy as

$$S_N^{(\alpha)} = \frac{1}{1-\alpha} \ln \left(\sum_{N_A} p^\alpha(N_A) \right). \tag{2.29}$$

Similarly, the limit $\alpha \to 1$ corresponds to the number entropy S_N and $\alpha = 0$ gives the Hartley number entropy.

Investigating scaling characteristics to distinguish various quantum phases led us to introduce the von Neumann entropy and its generalized form, Rényi entropies. These entropies have sensitivity for correlation and formation of states. In Rényi entropies, the α value also plays a role in the scaling. For instance, the Hartley entropy, $\alpha = 0$, is sensitive to configurations with low probability. The number entropy, or the generalized form, Rényi number entropies are sensitive to particle fluctuations between the subsystems. In our study, we highly benefit from studying the scaling in the entropies framework to detect thermalization or its breakdown in isolated quantum systems.

Chapter 3

Diffusion to Localization

The post-quench dynamics in a closed quantum system depend on interactions and disorder strength. In a clean system, a system with no disorder, particles and excitations propagate through the system ballistically, and the entanglement entropy S grows linearly in time t. Introducing disorder can alter this behavior and can lead to diffusion, where the motion of particles and excitations becomes more random and slower. Thermalization in such systems occurs when energy and information are spread evenly throughout the system over time. This progression can slow down for stronger disorder strength, leading to the prevention of particle or excitation transport, failure of thermalization, and resulting in localization. Localization is a topic of interest in disordered systems. One might ask how it is possible that, in some cases, after applying disorder to the system, instead of diffusion, the system experiences suppression of particle transport. Disorder manifests itself as random variations in system parameters, such as the potential in tight-binding models and its impact depends on whether the system is treated as a collection of particles or waves. Applying disorder to a system disrupts the coherent propagation of particles or waves and leads to scattering, interference, and, under certain conditions, localization. In non-interacting systems, this phenomenon is known as Anderson localization. Many-body localization is an extension of Anderson localization, also caused by the absence of diffusion; however, as the term suggests, it refers to the localization of a system with many interacting particles. Here, we explore the transition from diffusion to localization after applying disorder. As mentioned above, one can analyze the effect of disorder from two perspectives: particle picture and wave picture. For weak disorder,

particle transport is often governed by Brownian motion and

$$\langle x^2(t)\rangle = 2Dt \tag{3.1}$$

where D is the diffusion coefficient. As shown, the mean squared displacement of a particle grows linearly with time and follows the classical diffusion law. In the presence of disorder, particle experiences scattering from the random potential. This behavior can be described by the diffusion equation

$$\frac{\partial \rho(x,t)}{\partial t} = D\nabla^2 \rho(x,t) \tag{3.2}$$

where $\rho(x,t)$ is the density function. The solution of Eq. (3.2) is a Gaussian distribution

$$\rho(x,t) = \frac{1}{\sqrt{4\pi Dt}} e^{-x^2/4Dt}, \tag{3.3}$$

which describes the symmetric spreading of the particle's position over time. However, as disorder increases, particle may go through regions of high potential, such as a potential well. Then, the distribution deviates from this Gaussian form, showing suppressed transport.

$$\langle x^2(t)\rangle \sim t^\alpha, \quad 0 < \alpha < 1 \tag{3.4}$$

At even stronger disorder, the particle may become trapped in these regions of the potential, leading to a complete breakdown of diffusion. In this localized regime, $\langle x^2(t)\rangle$ saturates entirely over time, corresponding to $\alpha = 0$.

The effects described here are rooted in classical mechanics, where scattering events dominate. Unlike classical particles, quantum particles can tunnel through barriers and interact with the disordered potential through interference effects. Interference, a wave phenomenon, is fundamental to localization. In quantum systems, particles are governed by wave mechanics and described by a wave function. Particle's wavefunction extends beyond the classically forbidden region due to the tunneling effect and in a periodic potential, it can be described by a plane wave that fulfills the Bloch condition.

$$\psi_k(x) = e^{ikx} u_k(x), \tag{3.5}$$

where $u_k(x)$ is a periodic function with the same periodicity as the lattice. However, when disorder is introduced into the system, the periodicity of the potential

is disrupted and Bloch waves are no longer the eigenstates of the Hamiltonian of the system, and interference effects appear. Here, the particle scatters at the random disorder potential $V(x)$ and is either transmitted or reflected. Each scattering causes a phase shift in the particle's wavefunction. The resulting wavefunction is a superposition of multiple scattered waves

$$\psi(x) = \sum_j A_j e^{i\phi_j x}. \tag{3.6}$$

where A_j and ϕ_j are the amplitude and phase of the j-th scattered wave, respectively. After many scattering events, these waves interfere. The interference can be constructive or destructive, depending on the relative phases of the waves.

The transition from diffusion to localization can be understood through the decay of the wave function in space. In a localized regime, the particle's wave function $\psi(x)$ no longer extends throughout the system but instead decays exponentially with distance

$$|\psi(x)|^2 \sim e^{-|x|/\xi}, \tag{3.7}$$

where ξ is the *localization length*, characterizing the spatial extent of the wave function. The localization length depends inversely on the disorder strength; stronger disorder results in a smaller ξ, indicating tighter confinement. This interplay between disorder and interference, where the wave function becomes localized and the transport ceases, is known as Anderson localization.

3.1 Anderson Localization

Philip W. Anderson proposed in 1958 that electronic diffusion can vanish in a sufficiently random potential, in the absence of any electron–electron interaction. In quantum mechanics, Anderson localization refers to a single-particle phenomenon where disorder in a system can cause the wave function of a particle to become localized in certain regions of space [1]. However, this concept does not take into account interactions between particles. Hamiltonian of such a system can be described

by the tight-binding model

$$\hat{H} = \sum_j [-J_j(|j\rangle\langle j+1| + |j+1\rangle\langle j|) + V_j|j\rangle\langle j|] \tag{3.8}$$

where j denotes the lattice site. V_j and J_j are the random disorder potential and hopping amplitude at site j. Suppose the particle is localized at site j_0 at $t = 0$. The state of the system for $t > 0$ evolves according to Schrödinger equation

$$\Psi(j,t) = \langle j|e^{i\hat{H}t}|j_0\rangle. \tag{3.9}$$

Using the eigenstate decomposition of $\hat{H}$, we get

$$\Psi(j,t) = \sum_{k=1}^{L} e^{-iE_k t}\phi_k(j)\phi_k^*(j_0), \tag{3.10}$$

where $\phi_k(j) = \langle j|k\rangle$ is the amplitude of the k-th eigenstate at site j. We can obtain the probability density to find the particle at site j at long times by time averaging

$$\rho(j) = \lim_{T\to\infty} \frac{1}{T}\int_0^T |\Psi(j,t)|^2\, dt. \tag{3.11}$$

By substituting Eq. (3.10), we get

$$\begin{aligned}\rho(j) &= \lim_{T\to\infty} \frac{1}{T}\int_0^T \sum_{k,k'} e^{-i(E_k - E_{k'})t}\phi_k(j)\phi_k^*(j_0)\phi_{k'}^*(j)\phi_{k'}(j_0)\, dt \\ &= \sum_{k,k'} \phi_k(j)\phi_k^*(j_0)\phi_{k'}^*(j)\phi_{k'}(j_0)\left[\lim_{T\to\infty}\frac{1}{T}\int_0^T e^{-i(E_k-E_{k'})t}\, dt\right].\end{aligned} \tag{3.12}$$

We assume that energy levels are non-degenerate, $E_k \neq E_{k'}$ for $k \neq k'$. The time average of the oscillatory term satisfies

$$\lim_{T\to\infty}\frac{1}{T}\int_0^T e^{-i(E_k-E_{k'})t}\, dt = \lim_{T\to\infty}\frac{e^{-i(E_k-E_{k'})T}-1}{-i(E_k-E_{k'})\,T} = \delta_{kk'},$$

so that only the diagonal terms, $k = k'$, survive in the long-time limit. Therefore,

$$\rho(j) = \sum_{k=1}^{L} |\phi_k(j)|^2 |\phi_k(j_0)|^2. \tag{3.13}$$

In an Anderson localized system, this density exhibits exponential decay with distance from the initial site j_0

$$\rho(j) \sim \exp\left(-\frac{|j - j_0|}{\xi}\right), \tag{3.14}$$

where, as introduced before, ξ is the localization length. Each eigenstate of the system is also localized and

$$|\phi_k(j)|^2 \sim \exp\left(-\frac{|j - j_k|}{\xi_k}\right), \tag{3.15}$$

where ξ_k is the localization length specific to the eigenstate k. One way to study localization, is to consider a system partitioned into two subsystems A and B, as in chapter 2. We define the probability of the particle being in A, given that it was initially localized at site j_0, as

$$\langle Q^{N_A} \rangle = \sum_{j \in A} \rho(j) = \sum_{j \in A} \sum_{k=1}^{L} |\phi_k(j_0)|^2 |\phi_k(j)|^2. \tag{3.16}$$

where N_A is the number of sites in subsystem A. In a fully localized system, $\langle Q^{N_A} \rangle$ approaches 1 if j_0 lies within A, i.e., at a distance much larger than the localization length ξ from the boundary (e.g., $j_0 \gg \xi$ if the boundary is at $j = 0$), and as long as $|A| \gg \xi$. Conversely, if j_0 is out of A, $\langle Q^{N_A} \rangle$ tends to 0. As demonstrated, analyzing such systems analytically is inherently challenging due to the random nature of disorder, which requires statistical averaging over multiple realizations. It becomes even more complex when studying the transition from localized to delocalized phases, particularly in higher dimensions. However, in one dimension, the Anderson localization problem can be solved rigorously. To address these challenges, scaling theory provides a powerful framework. Rather than analyzing individual states or specific disorder configurations, scaling theory focuses on how localization properties evolve with system size and disorder strength.

3.1.1 Scaling Theory

In the case of non-interacting systems, scaling theory can explain how the transition from diffusion to localization happens. As mentioned above, the effect of dimensionality on Anderson localization is profound. In one- and two-dimensional systems, any amount of disorder leads to localization. In three dimensions, a critical disorder strength separates localized states from extended states. The scaling theory of localization, first put forward by Abrahams et al. [29], offers a general framework that explains this transition in disordered systems. In this study, the localization length and system size are related to the dimensionless conductance g. The dimensionless conductance g for electronic states in different dimensions is defined as

$$g = \frac{G}{e^2/h}, \tag{3.17}$$

where G is the conductance of the system. Alternatively, in disordered systems, g can also be expressed in terms of the transmission T,

$$g(L) = \frac{T(L)}{1 - T(L)}. \tag{3.18}$$

Depending on the value of g, the system is either in a localized or extended phase.

- For $g \gg 1$, the system is a conductor and the states are extended.
- For $g \ll 1$, the system is an insulator and the states are localized.

The scaling hypothesis states that the function g as a function of the system size L obeys a universal scaling law described by the beta function

$$\beta(g) = \frac{\mathrm{d} \ln g}{\mathrm{d} \ln L}. \tag{3.19}$$

The function $\beta(g)$ describes how g behaves as the system size is changed, whether the system is heading towards localization or delocalization when the thermodynamic limit is reached. The scaling theory predicts the different behaviors of $\beta(g)$ depending on the system's dimensionality d.

- $d \leq 2$**:** For all levels of disorder, $\beta(g) < 0$, meaning that g decreases with increasing L. This suggests that even the slightest disorder results in localization,

in agreement with the original predictions by Anderson.

- $d = 3$**:** There is a clear critical conductance g_c such that, for $g > g_c$, it is shown that $\beta(g) > 0$, implying the system exhibits extended states, and for $g < g_c$, it holds that $\beta(g) < 0$, resulting in localization.

The critical value g_c marks the Anderson transition, separating localized from extended states. At the critical point, the localization length ξ diverges as the disorder strength D approaches the critical value D_c,

$$\xi \sim |D - D_c|^{-\nu}, \tag{3.20}$$

where ν is the critical exponent. This exponent is a universal quantity that depends only on the dimensionality of the system and its symmetry class. Experimental and numerical studies suggest $\nu \approx 1.57$ for three-dimensional systems in the orthogonal universality class [30]. The predictions of scaling theory have been confirmed in many experimental studies. For example, experiments on ultracold atoms in optical lattices have managed to observe the critical disorder strength relevant for the Anderson transition. Similarly, measurements of electronic conductance in disordered semiconductor systems have exhibited scaling behavior consistent with theoretical predictions [31].

3.1.2 Scaling of Entanglement and Number Entropy

The studies of scaling behaviors of entanglement entropy and number entropy are used as analytical tools to distinguish phases and transport in systems that manifest Anderson localization. We can rewrite the Hamiltonian in Eq. (3.8) as

$$\hat{H} = -\sum_j J(\hat{c}_j^\dagger \hat{c}_{j+1} + h.c.) + \sum_j V_j \hat{n}_j, \tag{3.21}$$

where J is a uniform hopping amplitude and $V_j \in [-D/2, D/2]$. For a bipartition of the system into subsystems A and B, the Rényi number entropy is described as Eq. (2.29). Consider $|A| = |B| = L/2$. In a single-particle system, both the entanglement and number entropies are equivalent, as they reflect the same distribution properties

of the particle across the subsystems. Thus,

$$\langle S^{\alpha} \rangle = \langle S_N^{\alpha} \rangle = \frac{1}{1-\alpha} [\ln \left(Q^{\alpha} + (1-Q)^{\alpha} \right)] \tag{3.22}$$

where $Q = Q^{N_A}$ is the probability to find a particle in the subsystem A when initially placed at j_0 at $t \to \infty$. For an extended state, Q approaches $\frac{1}{2}$ as the probability for a single particle to be located either in subsystem A or B is the same. Thus, in the limit of $\alpha \to 1$, $\langle S_N^{\alpha} \rangle = \langle S_N \rangle$, and one can say that entropy grows to its maximum value, $\ln 2$. On the other hand, for the localized state, Q stays close to either 0 or 1, resulting in a lower entropy close to 0. However, the entropy value never will be exactly zero since quantum tunneling allows a small probability for particles to explore the cutoff region. In one and two dimensions, all the states are spatially localized for any $D > 0$. However, in 2D, the localization length ξ can grow significantly for weak disorder and Q may deviate slightly from extremes, leading to slightly higher entropies compared to 1D systems. In three-dimensional systems, the interplay between disorder strength D and the critical disorder strength D_c determines the phase and scaling behavior of entropy. For $D < D_c$, the system is in the extended phase,and for $D > D_c$, the system transitions into the localized phase. We can extend the idea of Anderson localization in a single-particle system to a many-particle non-interacting system. Here, scaling of the entanglement and number entropies become more useful for distinguishing transition. Since there is no interaction, we can analyze the system as a collection of evolving wavefunctions with disorder dictating the extent of localization. Consider the Hamiltonian in Eq. (3.21) in three dimensions.

$$\hat{H} = \sum_{\langle i,j \rangle} \left[-J \left(\hat{c}_i^{\dagger} \hat{c}_j + \text{h.c.} \right) \right] + \sum_j V_j \hat{n}_j, \quad \{\hat{c}_j, \hat{c}_n^{\dagger}\} = \delta_{j,n} \tag{3.23}$$

For weak disorder, particles retain significant mobility, wavefunctions can spread across the system, and entropies grow as

$$S \sim \sqrt{t},\ S_N \sim \frac{1}{4} \ln t. \tag{3.24}$$

This is known as the metallic regime in Anderson metal-insulator transition [32]. As we increase the disorder, subdiffusive transport emerges and entropy scaling shifts

toward a slower power law [32]

$$S \sim t^{\mu},\ S_N \sim \frac{\mu}{2} \ln t. \tag{3.25}$$

When D approaches D_c, the system enters a critical state where many states exhibit localization.

$$S \sim \ln t,\ S_N \sim \ln \ln t. \tag{3.26}$$

For $D > D_c$, we reach to the insulating regime, and entropies become constant which indicates localization and transport suppression. As we can see, Eq. (3.24), (3.25), and (3.26) are consistent with

$$S_N \sim \frac{1}{2} \ln S + c. \tag{3.27}$$

Numerical simulations explicitly verify this relation in the context of quench dynamics for free fermionic systems. In the free fermion case, it can also be proven analytically [33].

3.2 Many-Body Localization

The quest for the stability of Anderson localization in the presence of interactions has been well explored since 1985 [2, 34, 35]. In many-body systems, interactions between particles offer new mechanisms, such as dephasing, which could potentially destabilize localization [2, 36, 37]. Thus, the challenge is to ask whether the localized regime still remains robust in spite of these interactions. This led to the phenomenon known as many-body localization (MBL). Dephasing is one of the processes that impact the transition from localization to thermalization and it describes the loss of quantum coherence due to interactions.

Strong and fast dephasing can occur in a regime where there is the rapid loss of coherence leading to thermalization. In a many-body quantum system, local interactions interfere with phase correlations between quantum states leading the system to thermal equilibrium, where $\hat{\rho}_A(t \to \infty)$ can be locally described by a Gibbs ensemble. In regimes of high effective temperatures, the strong dephasing effects have the tendency of suppressing quantum phenomena significantly. In contrast, weak and slow dephasing can occur where interactions perturb localization in a more subtle

manner, resulting in a gradual increase of entanglement. Consider a model with two particles initially localized in separate subsystems and at a distance d of each other. The interaction[1] part of the Hamiltonian of the system can be written as

$$\hat{H}_I = \sum_{i\in A, j\in B} V \hat{n}_i \hat{n}_j, \tag{3.28}$$

since one particle is localized in subsystem A and the other in subsystem B. To ease the calculation, let us assume the system has four sites, the first two of them contributed to subsystem A and the last two to B. Thus, by using

$$\hat{n}_i = \hat{c}_i^\dagger \hat{c}_i,\ \tilde{d}_i^\dagger = \frac{1}{\sqrt{2}}(\hat{c}_i^\dagger + \hat{c}_{i+1}^\dagger) \text{ for } i = 1,\ 3\ , \tilde{d}_i^\dagger = \frac{1}{\sqrt{2}}(\hat{c}_{i-1}^\dagger - \hat{c}_i^\dagger) \text{ for } i = 2,\ 4, \tag{3.29}$$

we can rewrite Eq. (3.28) as

$$\hat{H}_I = \frac{V}{4} \sum_{\substack{k,k'=\{1,2\} \\ l,l'=\{3,4\}}} \tilde{d}_k^\dagger \tilde{d}_{k'} \tilde{d}_l^\dagger \tilde{d}_{l'}. \tag{3.30}$$

This basis transformation is adapted from the method presented in the Ph.D. thesis of Kiefer-Emmanouilidis [38]. Here, the interactions described by $\hat{H}_I$ assume that the particles are very close. However, if they are separated by a large distance d, their exponentially decaying wave function tails lead to a weaker interaction which can be expressed as

$$V \to C_{kl} V e^{-d/\xi} \delta_{k,k'} \delta_{l,l'}, \tag{3.31}$$

where C_{kl} depends on the localization properties of the single-particle orbitals. The localized nature of the eigenstates implies that in the absence of interactions, the system exhibits only oscillatory dynamics within each subsystem, without entanglement between them. The time-evolved state can be written as a superposition of eigenstates,

$$|\Psi(t)\rangle = \frac{1}{2} \sum_{\substack{k=\{1,2\} \\ l=\{3,4\}}} e^{-iE_{kl}t} \tilde{d}_k^\dagger \tilde{d}_l^\dagger |0\rangle, \tag{3.32}$$

[1]In earlier sections, the symbol V was used to denote disorder strength. However, starting from this section, V denotes the interaction strength and D refers to the disorder strength.

with energy

$$E_{kl} = \varepsilon_k + \varepsilon_l + \delta E_{kl}, \tag{3.33}$$

where δE_{kl} is the interaction-induced energy shift. By tracing out subsystem B, the reduced density matrix of A takes the form

$$\hat{\rho}_A = \frac{1}{2}\begin{pmatrix} 1 & F(t)/2 \\ F^*(t)/2 & 1 \end{pmatrix}, \tag{3.34}$$

where the off-diagonal elements oscillate as

$$F(t) = e^{-i\Omega t}(1 + e^{-i\delta\Omega t}), \tag{3.35}$$

with $\delta\Omega$ determined by energy differences due to interactions. Over time, the oscillations decay, leading to maximal mixing at times $t = (2n+1)\pi/\delta\Omega$, indicating dephasing. Here, we examined a system with no disorder. In a more general setting with disorder, the relaxation process gradually extends the wave functions, allowing for increasing overlap between them. This causes a slow growth of the entanglement region, which can be approximated as

$$x(t) \sim \xi \ln(Vt). \tag{3.36}$$

Thus, the entanglement entropy follows

$$S \sim x(t) \sim \xi \ln(Vt), \tag{3.37}$$

which differentiates many-body localization from Anderson localization, in which entanglement remains constant. For clearer insights into the interplay between interactions and disorder under many-body localization, we proceed to introduce the short-range fermionic J-V model in one dimension. The model presents a convenient starting point to argue about the role of interactions and disorder in the transition. The Hamiltonian of the J-V model is given by

$$\hat{H}_{J-V} = \sum_{j=1}^{L}[-J(\hat{c}_j^\dagger \hat{c}_{j+1} + h.c.) + V\hat{n}_j\hat{n}_{j+1} + D_j\hat{n}_j]. \tag{3.38}$$

It must be mentioned that the symbol V in the preceding chapter was utilized to

indicate the random disorder potential. In the present instance, though, V characterizes the short-range interaction strength, and D_j denotes a random on-site disorder potential drawn from a uniform box distribution, $D_j \in [-D/2, D/2]$. This model can be mapped to the spin-1/2 Heisenberg XXZ chain through a Jordan-Wigner transformation and $\hat{S}_j^z = \hat{n}_j - 1/2$, making it ideally suited for the investigation of localization phenomena in interacting spin systems.

$$\hat{H}_{XXZ} = \sum_j 2J(\hat{S}_j^x \hat{S}_{j+1}^x + \hat{S}_j^y \hat{S}_{j+1}^y + \Delta \hat{S}_j^z \hat{S}_{j+1}^z) + \sum_j W_j \hat{S}_j^z]; \; W_j \in [-W, W] \quad (3.39)$$

By setting $J = 1$, parameters V and D_j in Eq. (3.38) are equivalent to 2Δ and $\frac{1}{2}W_j$, parameters in Eq. (3.39), respectively. The system is initially prepared in a product state, and disorder is introduced at $t = 0$. The subsequent unitary evolution under $\hat{H}_{J-V}$ allows us to examine how entanglement and thermalization evolve over time. Introducing interactions ($V \neq 0$) is expected to enable dephasing processes. At weak disorder, interactions induce rapid dephasing, allowing the system to relax towards thermal equilibrium. However, it has been argued that as D increases, disorder disrupts the transport of quantum information, leading to a phase where many-body localization emerges, and the transition between thermal and MBL phases occurs at a critical disorder strength D_c, which has been subject to extensive studies. Estimates for the transition point vary, with values such as $D_c \approx 3.72$ for $V = 2$ [39], and some studies suggesting that an ergodic phase persists even for disorder strengths up to $D_c \sim 80$ [40]. More radical perspectives propose that in certain models, $D_c \to \infty$ [41, 4], implying that ergodicity might persist and the system never localizes.

3.2.1 Diagnostics of MBL

In this J-V model, the growth of the entanglement in the MBL phase is believed to be given by the equation derived previously, Eq. (3.37). Finite-size studies [42, 43, 44] also confirmed that such logarithmically increasing disorder-induced entanglement is accompanied by a point of saturation that scales with the length of the subsystem. However, it is important to distinguish between the entanglement entropy of eigenstates and that of states reached after a quench. The entanglement scaling of eigenstates can be understood by considering a system divided into two subsystems, A and B. If we turn off the coupling between these two subsystems, states are ten-

sor product states, $|\psi\rangle_{AB} = |\alpha\rangle_A \otimes |\beta\rangle_B$. Introducing an interaction term between subsystems and turning the coupling back on, which is localized near the boundary, perturbs the eigenstates but only within ξ. As a result, entanglement only develops locally near the boundary and grows only with the volume of the boundary $S \sim |\partial A|$ [43]. In quench dynamics, in contrast to a single eigenstate satisfying the area law, a superposition of eigenstates can give rise to a volume law of entanglement $S(\infty) \sim |A|$ [43, 44]. This is because entanglement entropy is a non-linear function in the state, i.e., the superposition rule cannot be applied straightforwardly.

The presence of an area-law entanglement implies that the MBL eigenstates can be linked to product states by a sequence of quasi-local unitary transformations [43]. The unitary operators deform the system to a basis where the Hamiltonian is diagonalized and comprises a set of local conserved quantities referred to as local integrals of motion (LIOMs). These conserved quantities guarantee that transport is blocked, yet permit weak interactions to facilitate slow phase shifts. To formalize this, consider the J-V model Eq. (3.38) in limit $J \to 0$. The Hamiltonian

$$\hat{H}_{J\to 0-V} = \sum_{j=1}^{L} [V \hat{n}_j \hat{n}_{j+1} + D_j \hat{n}_j] \tag{3.40}$$

commutes with $\hat{n}_j$ in every site, and the eigenstates are product states in occupation number basis $|\hat{n}_1, \hat{n}_2, ..., \hat{n}_L\rangle$. Now, each site has an effective local conserved quantity $\hat{n}_j$. When we turn on the weak interaction, $J \neq 0$, and assuming the system remains in the MBL phase, the Hamiltonian is no longer diagonal in occupation number basis. The above argument for the area-law entanglement implies that we can obtain new eigenstates from the product states $|\hat{n}_1, \hat{n}_2, ..., \hat{n}_L\rangle$ by a quasi-local unitary transformation, which diagonalizes the Hamiltonian. This transformation can be expressed as a product of quasi-local unitary operators, denoted by $\hat{U} = \prod_i \hat{U}_i$. Thus, in the new eigenbasis created, we have a new set of quasi-local integrals of motion labeled as $\hat{\tau}_j = \hat{U}^\dagger \hat{n}_j \hat{U}$. These operators $\hat{\tau}_j$ possess approximate spatial locality, i.e., each $\hat{\tau}_j$ is localized primarily near site j, with exponentially decaying contributions from other distant sites. Since $\hat{\tau}_j$ commutes with the full Hamiltonian Eq. (3.38), the system cannot fully thermalize under unitary evolution and interaction between LIOMs induce slow dephasing dynamic. We can rewrite the Hamiltonian Eq. (3.38) by using

LIOMs and obtain the effective form

$$H = \sum_i \epsilon_i \hat{\tau}_i + \sum_{i,j} J_{ij} \hat{\tau}_i \hat{\tau}_j + \sum_{i,j,k} V_{ijk} \hat{\tau}_i \hat{\tau}_j \hat{\tau}_k + \dots . \tag{3.41}$$

Here, ϵ_i are local energy shifts, J_{ij} describes interactions between localized operators, exponentially decreasing with distance, and V_{ijk} describes higher-order interactions. The weak couplings $J_{ij} \sim e^{-\frac{|i-j|}{\xi}}$ are responsible for the dephasing dynamics.

A diagnostic of the many-body localization transition, in addition to the study of entanglement dynamics, can be the statistical properties of the energy spectrum. In an ergodic thermalizing system, small perturbations cause strong mixing of eigenstates, leading to level repulsion and Wigner-Dyson statistics. The probability distribution of level spacings $p(s)$, where $s_\alpha = E_{\alpha+1} - E_\alpha$ is the difference between consecutive eigenenergies, follows the Wigner-Dyson distribution

$$P(s) = A_\beta s^\beta e^{-B_\beta s^2}, \qquad s \geq 0, \tag{3.42}$$

where $\beta = 1, 2, 4$ depends on the symmetry class of the Hamiltonian. For small s, this gives $P(s) \propto s^\beta$, reflecting level repulsion, while for large s the distribution decays approximately Gaussian. This behavior was observed in thermalizing many-body lattice models, confirming their chaotic behavior and ergodicity [34]. In contrast, in the MBL phase, an extensive set of quasi-local integrals of motion emerges, preventing eigenstate mixing and leading to Poisson statistics

$$P(s) = e^{-s}, \qquad s \geq 0, \tag{3.43}$$

which describes a system with independent and uncorrelated energy levels [43]. Unlike the Wigner–Dyson case, $P(0) \neq 0$, meaning there is no level repulsion. This Wigner-Dyson to Poisson crossover has been observed numerically and experimentally. Early numerical studies by Oganesyan and Huse [34] and Pal and Huse [45] demonstrated that at weak disorder, level statistics are Wigner-Dyson statistics, while for stronger disorder strength, level repulsion disappears, and the level statistics become Poissonian. They established that in Eq. (3.39), the transition happens at a critical disorder strength $W_* \approx 3.5$ for $J = 1/4$, which marks the boundary between the thermal and MBL phases. This spectral transition is a result of the emergent integrability property of the MBL phase.

Another diagnostic method for the distinction of many-body localized phases from ergodic phases can be fidelity measurements, which are commonly explored through the Loschmidt echo. Loschmidt echo quantifies how a quantum state is sensitive to perturbations and its behavior depends on in what regime the systems is, localizing or thermalizing. Loschmidt echo is a special case of time-dependant fidelity and finds the overlap between a quantum state and its time-evolved counterpart under a perturbed Hamiltonian and is expressed as

$$S(t) = \langle \psi_0 | e^{iHt} e^{-iH_0 t} | \psi_0 \rangle, \tag{3.44}$$

where H_0 is initial Hamiltonian and H is the quench Hamiltonian. In ergodic phases, the Loschmidt echo exhibits exponential decay, a hallmark of chaos and fast loss of information. However, many-body localized phases show power-law decay in Loschmidt echo fluctuations, which ultimately saturates at a value that falls off exponentially with system size. This slow decay is a consequence of local integrals of motion, which preserve memory of the initial state and prevent full thermalization [46]. The Loschmidt echo fluctuations in MBL systems are helpful in detecting dephasing dynamics due to interaction between localized orbitals [47].

3.2.2 Scaling of Number Entropy and the Debate

The number entropy has also been investigated under the framework of many-body localization as a diagnostic to approximate localization and suppression of particle transport. Initial numerical and analytical investigations focused on its evolution behavior in systems predicted to exhibit MBL, particularly how it compares to entanglement entropy and particle-number fluctuations. The first numerical studies of entanglement entropy in the context of MBL were conducted by Znidaric et al. (2008) [48], where they identified logarithmic growth of entanglement entropy, as $S = \ln t$, in suggested MBL systems. This was subsequently confirmed by a study conducted by Bardarson et al. (2012) [22], where the analysis was furthered to particle-number fluctuations, expressed as ΔN^2, and found that these fluctuations tend to saturate, in contrast to the unbounded logarithmic growth of entanglement entropy. These results provided numerical evidence for distinguishing localized from ergodic phases and formed the foundation for interpreting slow entropy growth as a signature of MBL.

The theoretical framework underlying these observations was formulated by Serbyn et al. [44] and Huse et al. [49], who put forward the idea of local integrals of motion (LIOMs). In this framework, it was assumed that in the MBL phase, transport of particles should be inhibited, resulting in restricted number fluctuations. Consequently, the number entropy will remain approximately constant. This understanding was used in the explanation of more numerical and experimental findings. Lukin et al. (2019) [50] measured number entropy in a quasi-periodically disordered system of interacting bosons. It was suggested that if number entropy saturates but entanglement entropy continues to grow logarithmically with time, the system is in an MBL phase. This argument was based on the idea that if particle-number fluctuations are pinned down, then number entropy will also become saturated. Experimental results kept open the possibility that number entropy could increase slowly, but without bound. Another development in the investigation of number entropy was the work of Kiefer-Emmanouilidis [33, 3, 28], a former student of Jesko Sirker, my supervisor on this thesis. His studies, both numerical and analytical results, revealed that in the putative MBL phase, number entropy follows a double logarithmic growth pattern

$$S_N \sim \ln S \sim \ln \ln(t). \tag{3.45}$$

This is a behavior that contradicts the expectation of the number entropy saturating in the many-body localized phase, thus putting into question the long-time stability of localization. The implication of the results of the study by Kiefer and co-authors is that if this scaling persists indefinitely, then MBL does not represent a truly localized phase in the thermodynamic limit. This view aligns with the arguments by Suntajs et al. (2020) [4], who also questioned the existence of MBL. While some studies had justified scaling $S_N \sim \ln \ln(t)$ as an inherent property of MBL, others had pointed out the behavior to be transient. Luitz and Bar Lev argued that number entropy should saturate at some point despite the entanglement entropy continuing to increase. The conclusion was based on numerical results that at strong disorder, system-size-independent values of number entropy saturation are reached. Kiefer's research also probed this aspect, demonstrating that for certain system sizes and strengths of disorder, number entropy can exhibit fluctuations rather than strict saturation. However, he found that the fluctuations can be accounted for by averaging over initial conditions, a feature even in Anderson localized systems.

The discussion on the stability of the many-body localized phase remains an open question. This has led to a further study of many-body localization in other settings. A specific model that has attracted significant attention in the study of many-body localization is the Aubry-André model. In the following chapter, I will present the Aubry-André model and its relevance to the study of many-body localization. This will be a prelude to presenting my results, building on earlier works involving the use of number entropy, Hartley entropy, and particle-number fluctuations as diagnostic tools in assessing the stability of MBL.

Chapter 4

Model and Method

4.1 Aubry-André model

In this thesis, we want to compare the quenched disorder case with the Aubry-André (AA) case. We will study the Hamiltonian Eq. (3.38) with D_j being the Aubry-André potential. The Aubry-André potential is periodic, however, it has a long periodicity so locally it does look like a disorder potential. The onsite potential is given by

$$D_j = D\cos(2\pi\beta j + \phi), \tag{4.1}$$

where D is disorder strength, β is a Diophantine number[1], typically chosen as the golden ratio $\beta = (1+\sqrt{5})/2$, and ϕ is a random phase offset, introduced to sample different disorder realizations. In contrast to the quenched disorder case, this form of Eq. (4.1) ensures that there will always be a potential difference between neighboring sites. In the quenched random case, one can by chance get several sites that have roughly the same potential and, therefore, act as thermalizing bubbles for the rest of the system. These bubbles lead to what is often called *avalanches*. This mechanism is crucial in distinguishing between true MBL and finite-size MBL effects [51].

The Aubry-André model is fully understood in the non-interacting case and is mathematically equivalent to the almost Mathieu operator. The time-independent Hamiltonian of this model is given by

[1] A number β is Diophantine if there exist constants $c > 0$ and $r > 1$ such that $|\sin(2\pi j\beta)| > \frac{c}{|j|^r}$ for all $j \neq 0$. Liouville numbers, as irrational numbers, do not satisfy this condition. If β is Liouville, meaning it is extremely well approximated by rationals, then the system does not undergo a sharp transition, and the spectrum remains singular continuous rather than pure point.

$$\hat{H} = \sum_j [-J(|j\rangle\langle j+1| + |j+1\rangle\langle j|) + D\cos(2\pi\beta j + \phi)|j\rangle\langle j|]. \tag{4.2}$$

Having studied this model, it has been rigorously proven that there exists a phase transition at a critical potential strength $D_c = 2J$ and for $D > 2J$, eigenstates become localized [52]. However, a necessary condition for the sharp transition is that β must be a Diophantine number [52], and a typical choice for it is the golden ratio, as mentioned above. We know that in the non-interacting case, the Aubry-André potential is less effective in localizing particles than quenched disorder since it allows for extended states at weak disorder $D < 2J$. Several reasons justify the choice of the AA model in the study of interacting systems. The Aubry-André potential is less studied theoretically in the interacting case; however, all the cold-atomic gas experiments are using this potential since it is easier to realize and control compared to random disorder [50]. On the theoretical side, a very recent paper by the das Sarma group [51] claims that MBL in quasi-periodic potentials, including Aubry-André, might be more stable than in the quenched disorder case. In a randomly disordered system, large thermal bubbles can emerge statistically in a sufficiently large system [5]. Once formed, these bubbles can grow indefinitely, destroying localization across the system. This suggests that MBL in random systems is at best a finite-size phenomenon, as increasing system size allows more thermal inclusions to form [5]. Unlike the random case, thermal bubbles in the AA model are constrained because the quasiperiodic potential limits the size of thermal regions. As a result, the avalanche mechanism is suppressed, making MBL in the AA model potentially more stable and more likely to survive in the thermodynamic limit [51]. In our studies, we also fix the potential difference between sites near the cut, ensuring that, regardless of system size, there are no accidentally resonant sites near the cut, which could otherwise mimic thermalizing bubbles.

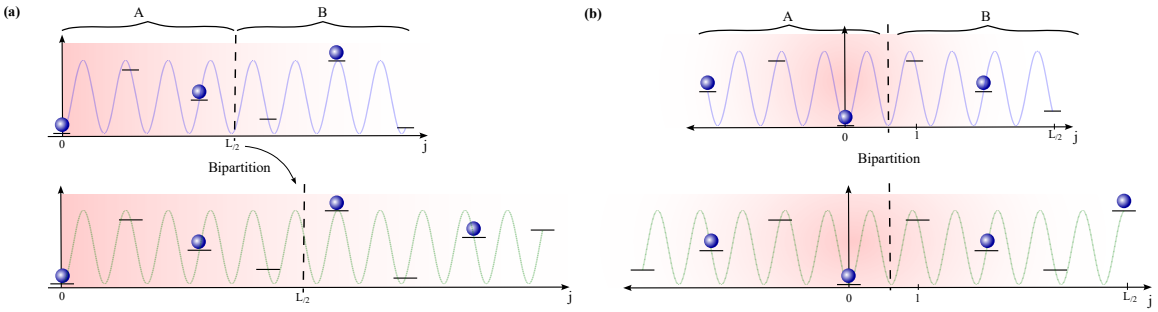

Figure 4.1: Sketch on reindexing sites to fix the potential difference across the cut. (a) In the original ordering, the potential difference depends on the system size L. (b) By reindexing, the cut always lies between $j = 0$ and $j = 1$, making it independent of L.

4.2 Methodology

Exact diagonalization is a numerical method to solve quantum many-body systems through direct computation of the eigenvalues and eigenvectors of the Hamiltonian matrix. It gives exact solutions in a finite Hilbert space and has been broadly used in studies of quantum thermalization and localization phenomena. However, there is a limitation while using this method and that is its exponential growth in computational complexity with system size. The Hilbert space for a quantum system with L sites grows as 2^L for spin-$\frac{1}{2}$ or spinless fermionic systems, and even faster for larger local Hilbert spaces. Trotter-Suzuki decomposition is a second method for studying larger systems.

4.2.1 Exact Diagonalization

Consider a Hamiltonian operator $\hat{H}$ and a chosen orthonormal basis $\{|\Phi_i\rangle\}$, which may represent occupation number states in fermionic systems or spin configurations in quantum spin models. The Hamiltonian matrix elements in this basis are given by

$$[H_\Phi]_{ij} = \langle\Phi_i|\hat{H}|\Phi_j\rangle, \tag{4.3}$$

where $\hat{H}$ is a Hermitian operator, and

$$[H_\Phi]_{ji} = [H_\Phi]^*_{ij}, \tag{4.4}$$

ensures real eigenvalues. A general state in this basis can be expressed as a linear combination

$$\hat{H}|\Phi_i\rangle = \sum_k C_{ki}|\Phi_k\rangle. \tag{4.5}$$

Thus, the corresponding matrix elements are

$$[H_\Phi]_{ji} = \sum_k C_{ki}\langle\Phi_j|\Phi_k\rangle = C_{ji} \text{ since } \langle\Phi_j|\Phi_k\rangle = \delta_{ik}. \tag{4.6}$$

To represent the Hamiltonian more compactly, we can introduce a vector of basis states,

$$\vec{\Phi} = [|\Phi_1\rangle, |\Phi_2\rangle, ..., |\Phi_N\rangle], N = 2^L; \tag{4.7}$$

then, the Hamiltonian matrix can be expressed as

$$\hat{H}_\Phi = \vec{\Phi}^\dagger \hat{H} \vec{\Phi} = \begin{bmatrix} \langle\Phi_1|\hat{H}|\Phi_1\rangle & \langle\Phi_1|\hat{H}|\Phi_2\rangle & \dots \\ \langle\Phi_2|\hat{H}|\Phi_1\rangle & \langle\Phi_2|\hat{H}|\Phi_2\rangle & \dots \\ \vdots & \vdots & \ddots \end{bmatrix}. \tag{4.8}$$

To diagonalize the Hamiltonian, we introduce an eigenbasis $\{|\Psi_i\rangle\}$ such that

$$\hat{H}|\Psi_i\rangle = E_i|\Psi_i\rangle. \tag{4.9}$$

Since the eigenbasis is orthonormal, $\langle\Psi_i|\Psi_j\rangle = \delta_{ij}$, we obtain the diagonal matrix representation

$$[H_\Psi]_{ji} = E_i\delta_{ji}. \tag{4.10}$$

Finding the eigenstates involves a basis transformation

$$|\Psi_i\rangle = \sum_k V_{ki}|\Phi_k\rangle, \tag{4.11}$$

where V is a unitary matrix satisfying $V^\dagger V = VV^\dagger = I$. The transformation from the original basis $\vec{\Phi}$ to the eigenstate $\vec{\Psi}$ can be expressed as

$$\vec{\Psi} = V\vec{\Phi} = [|\Psi_1\rangle, |\Psi_2\rangle, ..., |\Psi_N\rangle], \tag{4.12}$$

and the Hamiltonian in the eigenbasis is given by the similarity transformation

$$\hat{H}_\Psi = V\hat{H}_\Phi V^\dagger. \tag{4.13}$$

If the system has a conserved quantity represented by an operator $\hat{X}$ that commutes with $\hat{H}$, $[\hat{H}, \hat{X}] = 0$, then we can classify states by a quantum number x such that

$$\hat{X}|x, i\rangle = x|x, i\rangle. \tag{4.14}$$

This allows us to define $\vec{\Phi} = [|x_1; 1\rangle|x_1; 2\rangle...|x_2; 1\rangle|x_2; 2\rangle...]$ and structure the Hamiltonian into block-diagonal form, where each block corresponds to a subspace of definite x

$$\hat{H}_\Phi = \begin{bmatrix} H_\Phi^{x_1} & 0 & 0 & \dots \\ 0 & H_\Phi^{x_2} & 0 & \dots \\ 0 & 0 & H_\Phi^{x_3} & \dots \\ \vdots & \vdots & \vdots & \ddots \end{bmatrix}. \tag{4.15}$$

Each block $H_\Phi^{x_i}$ can then be diagonalized separately,

$$\hat{H}_\Psi^{x_i} = V^{x_i}\hat{H}_\Phi^{x_i}(V^{x_i})^\dagger. \tag{4.16}$$

Thus, exact diagonalization allows us to solve for the eigenvalues and eigenvectors of large Hamiltonians by exploiting symmetries and block structures in the system. An example of block diagonalization is the total particle number operator $\hat{N} = \sum_{j=1}^{L} \hat{n}_j$. If $\hat{N}$ commutes with $\hat{H}$, i.e. $[\hat{H}, \hat{N}] = 0$, then the Hilbert space can be decomposed into subspaces of fixed particle number N, with $\hat{N}|\Psi_i\rangle = N|\Psi_i\rangle$. This enables us to restrict $\hat{H}$ to a subspace of fixed particle number N. For fermionic lattice models, Hamiltonians can be constructed in the occupation number basis as described by Eq. (3.38), and the fermionic annihilation (creation) operators fulfill the anti-commutation relations

$$\left\{\hat{c}_i^{(\dagger)}, \hat{c}_j^{(\dagger)}\right\} = 0, \ \left\{\hat{c}_i, \hat{c}_j^\dagger\right\} = \delta_{ij}. \tag{4.17}$$

The corresponding number operator at each site is defined as $\hat{n}_j = \hat{c}_j^\dagger \hat{c}_j$. Each lattice site can be treated as a two-level system, and the full Hilbert space is constructed by taking tensor products over all sites. The total Hamiltonian $\hat{H}_\Phi$ can then be built using matrix representations of these operators according to the chosen model, hopping terms, interactions, and on-site potentials. To restrict the Hamiltonian to the N-particle subspace, we define a projection matrix P^N, whose rows are the basis states $\Phi_i \in \mathcal{H}_N$ with $\hat{N}|\Phi_i\rangle = N|\Phi_i\rangle$. This selects only the configurations with exactly N particles, and we get

$$\hat{H}_\Phi^N = P^N \hat{H}_\Phi (P^N)^\dagger, \tag{4.18}$$

which reduces the dimensionality from 2^L to $\binom{L}{N}$. Once the Hamiltonian is reduced, time evolution can be performed using

$$\hat{U}(t) = \exp\left(-i\hat{H}_\Phi^{(N)} t\right). \tag{4.19}$$

4.2.2 Trotter-Suzuki Decomposition

Trotter-Suzuki decomposition is an alternative method to approximate quantum dynamics in larger quantum many-body systems, where exact diagonalization fails. In Eq. (4.19), if the Hamiltonian consists of non-commuting terms, direct exponentiation is not very feasible. This method provides the approximation by splitting the Hamiltonian into two or more parts so that we can exponentiate them separately [53, 54]. For a Hamitonian composed of $\hat{H} = \hat{H}^A + \hat{H}^B$, where $\hat{H}^A$ and $\hat{H}^B$ do not necessarily commute, a second-order trotter expansion approximates time evolution for a small time step δt as

$$\hat{U}(\delta t) = e^{-i(\hat{H}^A + \hat{H}^B)\delta t} = e^{-i\hat{H}^A \delta t/2} e^{-i\hat{H}^B \delta t} e^{-i\hat{H}^A \delta t/2} + \mathcal{O}(\delta t^3), \tag{4.20}$$

where the error $\mathcal{O}(\delta t^3)$ for a sufficiently small time step can be ignored. $\hat{H}^A$ and $\hat{H}^B$ could correspond to two parts of the Hamiltonian acting on even and odd sites of the lattice.

$$\hat{H}^A = \sum_{j=1}^{L/2} \hat{H}_{2j-1,2j}, \quad \hat{H}^B = \sum_{j=1}^{L/2-1} \hat{H}_{2j,2j+1}. \tag{4.21}$$

By using these even and odd Hamiltonians in Eq. (4.20), we get

$$\hat{U}(\delta t) = \prod_{j=1}^{L/2} e^{-i\hat{H}_{2j-1,2j}\delta t/2} \prod_{j=1}^{L/2-1} e^{-i\hat{H}_{2j,2j+1}\delta t} \prod_{j=1}^{L/2} e^{-i\hat{H}_{2j-1,2j}\delta t/2} + \mathcal{O}(\delta t^3), \tag{4.22}$$

which represents the second-order Trotter-Suzuki approximation for systems with alternating two-site interactions.

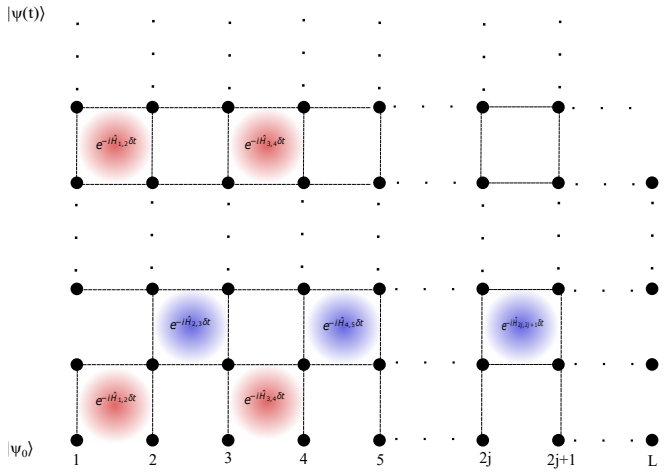

Figure 4.2: A simple illustration of the second-order Trotter-Suzuki decomposition.

Chapter 5

Results

In this section, I present our results for a one-dimensional, half-filled lattice with L sites. For the investigation of the Aubry-André model, we consider the standard fermionic representation of the J-V model with $J = 1$ for the system constructed of two equal subsystems, and we start from a Neel state with each subsystem containing half of the particles. The total number of particles in the system is conserved. Our study is mainly governed by analyzing the time evolution of the number entropy and its relation to entanglement entropy. Additionally, we examine the Hartley number entropy for the cases where the number entropy is not sufficiently sensitive to the small fluctuations around the cutoff. All simulations are performed numerically using Python®. In each simulation, we sample over 2000 disorder realizations, generated by varying both ϕ and β. We use 400 values of $\phi \in [0, \pi]$ and 5 Diophantine values of β, including the golden, silver, and bronze ratios, π, and Euler's number.

Our results for the time evolution of the number entropy are largely consistent with those obtained in the quench disorder case studies. We find that the relationship between entanglement entropy and number entropy follows $S_N \sim \ln S$, in agreement with the previous studies [3, 55]. As shown in Fig. 5.1, the entanglement entropy scales with $S \sim \ln t$, as expected, while the number entropy scales with $S_N \sim \ln \ln t$, leading to relation $S_N \sim \ln S$. Similarly to the case of quenched disorder, we do not observe a fast saturation of number entropy as expected for the localized regime, where particle transport is suppressed. This indicates that number entropy continues to grow until the entanglement entropy saturates and is in agreement with previous studies claiming that the MBL phase may not persist in the thermodynamic limit

[4]. In Fig. 5.1(c), the inset shows the deviation times t_d for both S and S_N. In our representation, we plot the deviation time as the time that the data deviates by a fixed threshold of 10% from fits. In a truly localized regime, we expect t_d for the number entropy to plateau with increasing system size while t_d for entanglement entropy increases with D. However, our results show that the deviation times for both entropies remain nearly parallel across all disorder strengths and this correlated behavior provides no clear sign of full localization. Instead, it suggests that both entropies continue to evolve together and saturate eventually, due to finite-size effects.

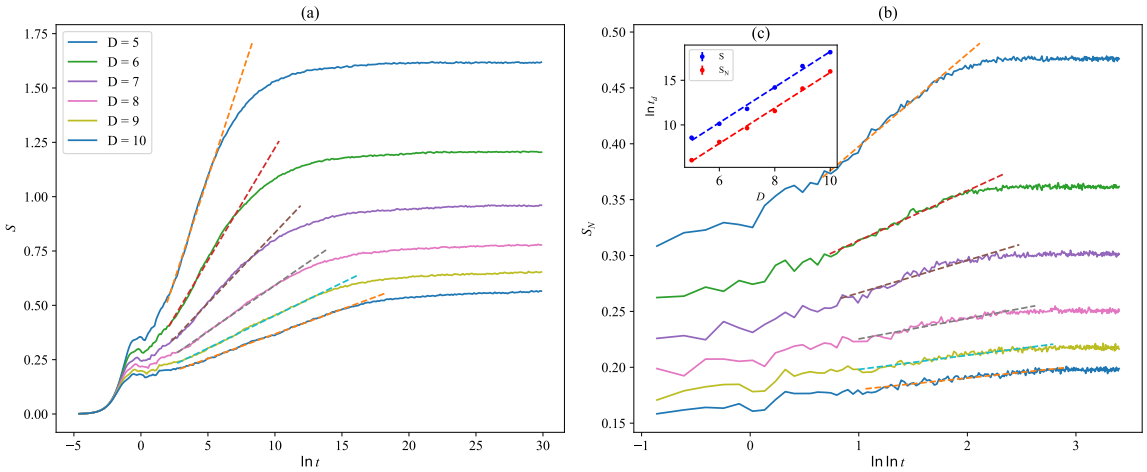

Figure 5.1: Time evolution of entanglement and number entropy for a system size $L = 16$, across various disorder strengths D. The initial state is a Néel state, and results are averaged over 2000 realizations. (a) Entanglement entropy S exhibits logarithmic growth over time, $S \sim \ln t$, with slower growth at higher strengths D, followed by finite-size saturation at long times. (b) Time evolution of the number entropy S_N scaling as $S_N \sim \ln \ln t$. The slower double-logarithmic growth compared to S suggests that S_N always grows slower than S. The inset (c) demonstrates the deviation times t_d for both S and S_N as a function of D.

The data in Fig. 5.1 are fitted with the functions $S = \mu \ln t$ and $S_N = \frac{\nu}{2} \ln \ln t$, where prefactors μ and ν are extracted as functions of disorder strength D for a system size $L = 16$, as shown in Fig. 5.2. As the disorder strength increases, these prefactors become smaller, indicating a suppression in the growth rates of entanglement and number entropy. This behavior also demonstrates that the scaling of entanglement entropy and number entropy are closely related and share a power-law dependence on the disorder strength. The prefactors μ and ν, as well as t_d in Fig. 5.1(c), were cal-

culated over multiple time intervals. However, the extracted values remained almost consistent across these variations, leading to error bars that are nearly invisible.

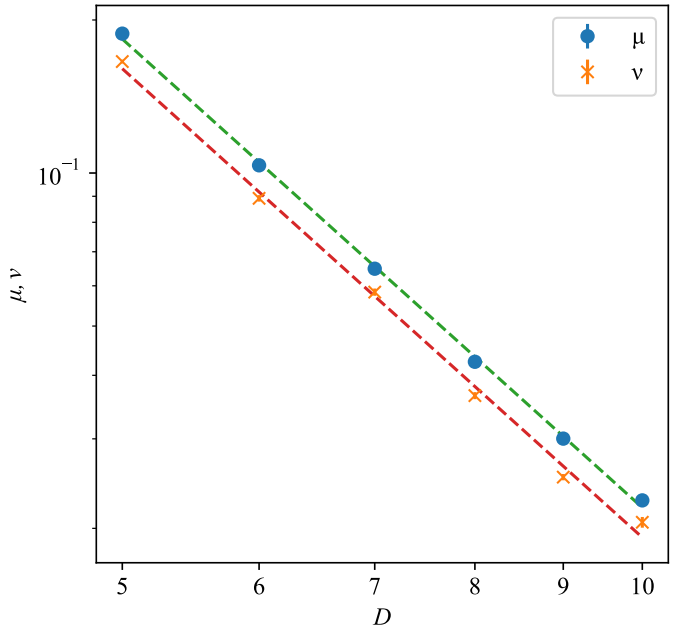

Figure 5.2: Scaling of the fit parameters μ and ν as functions of the disorder strength D. The parameter μ quantifies the growth rate of the entanglement entropy S as it scales as $\mu \ln t$, and ν quantifies the growth rate of the number entropy S_N, scaling as $\frac{\nu}{2} \ln \ln t$. Both parameters illustrate power-law scaling with respect to D. While this indicates that although increasing disorder suppresses the dynamics of both entropies, the scaling behavior remains correlated, following μ and $\nu \sim D^{-\alpha}$ with exponent $\alpha \simeq 3.06$.

In our studies, within the number entropy, there are two different averages that we can examine; one is to compute the entropy from the averaged particle number distribution and the other is to compute the entropy for each separate realization and then average over all realizations. We explain the relationship between the two methods via Jensen's inequality. Let $\{p_n^{(i)}\}$ denote the particle number distribution for the i-th disorder realization, with $i = 1, \ldots, R$, where R is the total number of disorder realizations which in our case is 2000. The averaged number entropy is given by

$$\bar{S}_N(p_n) = \frac{1}{R} \sum_{i=1}^{R} S_N(p_n^{(i)}) = \frac{1}{R} \sum_{i=1}^{R} \sum_{n} \left(-p_n^{(i)} \ln p_n^{(i)} \right). \tag{5.1}$$

On the other hand, the number entropy computed from the averaged particle number distribution $\bar{p}_n = \frac{1}{R}\sum_{i=1}^{R} p_n^{(i)}$ is

$$S_N(\bar{p}_n) = \sum_n \left(-\bar{p}_n \ln \bar{p}_n\right). \tag{5.2}$$

To establish a relation between these two quantities, we use Jensen's inequality for the concave function $f(x) = -x \ln x$, by fixing n and defining $x_i = p_n^{(i)}$, with equal weights $\omega_i = \frac{1}{R}$. Then,

$$\frac{1}{R}\sum_{i=1}^{R}\left(-p_n^{(i)} \ln p_n^{(i)}\right) \leq -\left(\frac{1}{R}\sum_{i=1}^{R} p_n^{(i)}\right) \ln\left(\frac{1}{R}\sum_{i=1}^{R} p_n^{(i)}\right) = -\bar{p}_n \ln \bar{p}_n. \tag{5.3}$$

By summing over all n, we obtain

$$\frac{1}{R}\sum_{i=1}^{R}\sum_n \left(-p_n^{(i)} \ln p_n^{(i)}\right) \leq \sum_n \left(-\bar{p}_n \ln \bar{p}_n\right), \tag{5.4}$$

or,

$$\bar{S}_N(p_n) \leq S_N(\bar{p}_n), \tag{5.5}$$

demonstrating that the number entropy of the averaged particle number distribution provides an upper bound on the averaged number entropy. Although one might expect $S_N(\bar{p}_n)$ to be smoother due to the averaging over realizations before applying the entropy function, which suppresses rare events, this is not what we observe in our data. In our numerical data, $S_N(\bar{p}_n)$ exhibits more fluctuations than $\bar{S}_N(p_n)$, however, remains an upper bound and, as it may not capture the typical behavior of the system, the averaged entropy $\bar{S}_N(p_n)$, better reflects the scaling of the number entropy, as shown in Fig. 5.3.

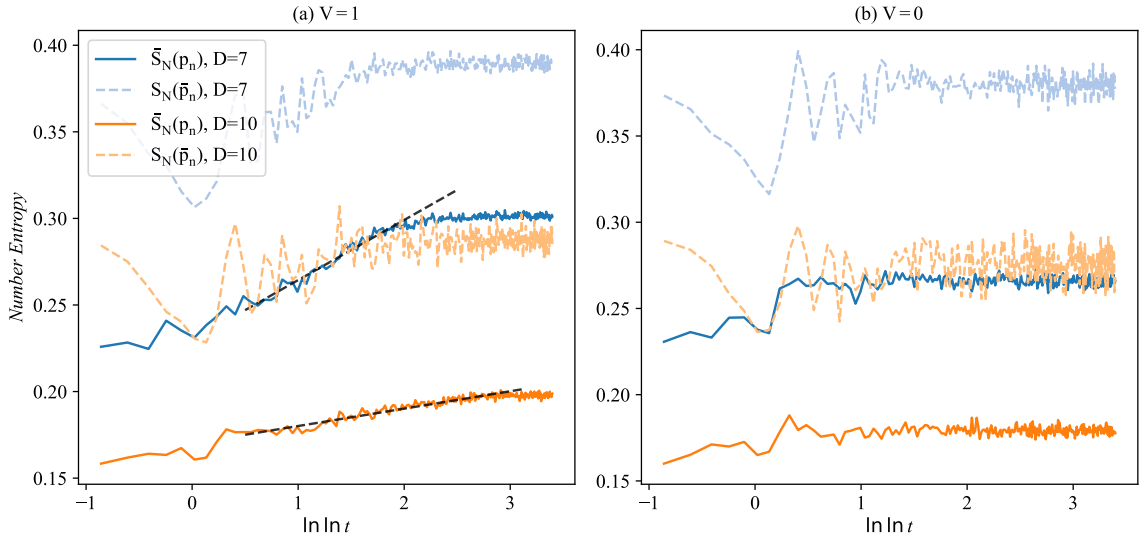

Figure 5.3: Comparison between the averaged number entropy $\bar{S}_N(p_n)$ (solid lines) and the number entropy computed from the averaged distribution $S_N(\bar{p}_n)$ (dashed lines), for disorder strengths $D = 7$ (blue) and $D = 10$ (orange), for interacting (a) $V = 1$ and non-interacting case (b) $V = 0$. Jensen's inequality guarantees that $\bar{S}_N(p_n) \leq S_N(\bar{p}_n)$.

Another way to analyze our data is to compare how the saturation values of the S and S_N scale with system size L for various disorder strengths, as shown in Fig. 5.4. In this figure, in the non-interacting case, we clearly observe that for weak disorder $D < 2$, the saturation value of S increases with L following a power-law trend, where all the single-particle states are delocalized and the system behaves ergodically. However, for $D \geq 2$, this growth starts to flatten, suggesting a transition to area-law scaling associated with Anderson localization at a critical value of $D_c = 2$. In contrast, the interacting case shows that the saturation values of both S and S_N continue to grow with L even at large disorder strengths. It should be emphasized that the low number of system sizes used in Fig. 5.4(b) and (c) might limit our analysis. For example, the behavior in the saturation values of S_N for disorder values $D = 7, 10$ in the MBL case, where the entropy initially increases and then decreases, might suggest a change in the power-law scaling. However, a similar trend appears in the non-interacting case and is likely attributable to even-odd effects. When the length of the subsystem $L/2$ is odd and such that one subsystem has an extra particle when starting from the Neel state, the entropies can fluctuate.

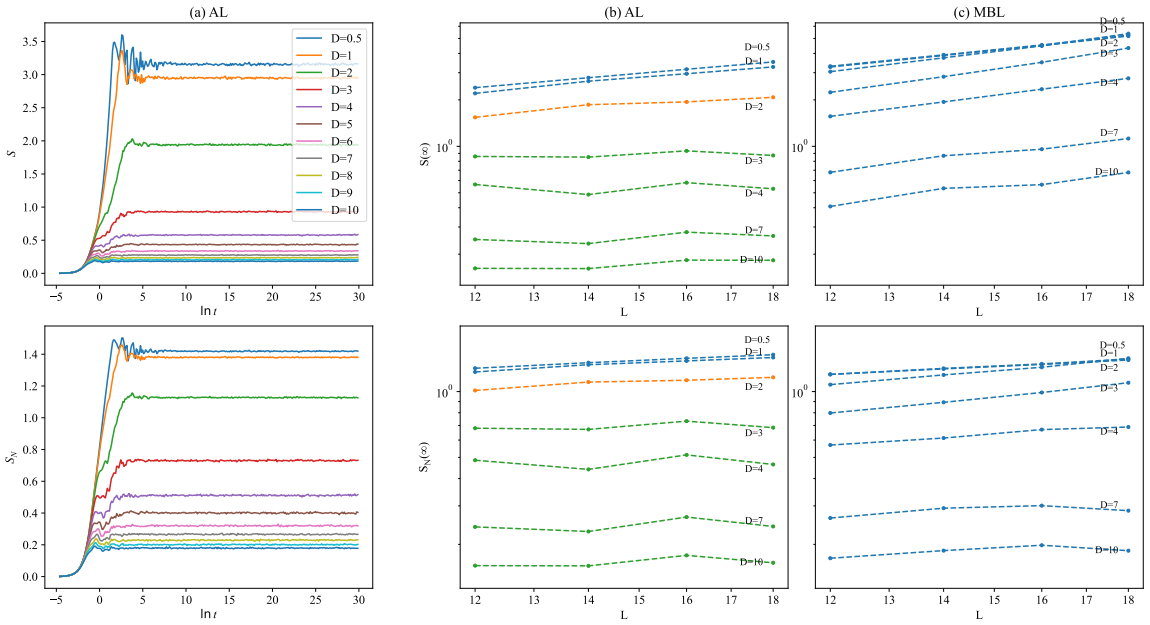

Figure 5.4: Time evolution of von Neumann and number entropy and saturation values of these entropies as a function of system size L for different disorder strengths D for both interacting and non-interacting cases. Columns (a) and (b) correspond to the case $V = 0$, and (c) to the case $V = 1$. In the non-interacting case, for $D < 2$, the saturation value exhibits a clear power-law scaling with L, indicating extended states and volume-law entanglement. However, for $D \geq 2$, this scaling behavior starts to break down, indicating localization. This suggests a critical disorder strength of $D_c \approx 2$ for the transition to the Anderson localized phase. In contrast, the interacting case still shows power-law scaling even for larger disorder values.

As discussed earlier, the Hartley number entropy $S_N^{(\alpha \simeq 0)}$ is also useful, as it captures rare events that may be too small to affect the number entropy S_N. It provides a more sensitive measure of how particle configurations spread across the cut during time evolution. In Fig. 5.5, which is for Anderson case, we observe a clear distinction between regimes. For weak disorder $D < 2$, the entropy shows volume-law behavior, growing with system size and exhibiting step-like features over time. These steps correspond to the particle transfer across the cut. The saturation value for all weak disorders below the transition is the same and corresponds to complete thermalization with all particle number configurations explored. In our half-filled system, this means every possible way of distributing $M = L/2$ particles between the two subsystems that occurs with non-zero probability. Then, the maximal Hartley number entropy is $S_N^{(\alpha \simeq 0)} = \ln(L/2 + 1)$. However, at the critical disorder strength $D_c = 2$,

the volume-law trend begins to break down, and for $D > 2$, only a limited range of particle-number configurations is explored and the entropy saturates rapidly to a value that does not scale with system size. This saturation is consistent with area-law behavior in Anderson localization. In the interacting case, Fig. 5.6, however, volume-law scaling persists even at higher disorder values, with $S_N^{(\alpha \simeq 0)}$ continuing to grow for $D = 3, 4, 7$. Only at very large disorder ($D = 10$) the entropy stops showing volume-law. Even then, instead of saturating fast, the curves show a slow growth, suggesting a scaling of $\ln \ln t$, similar to that observed in the number entropy S_N. In other words, the system is not fully localized and there is ongoing but extremely slow transport of particles between the subsystems, so that some new number configurations are explored over time.

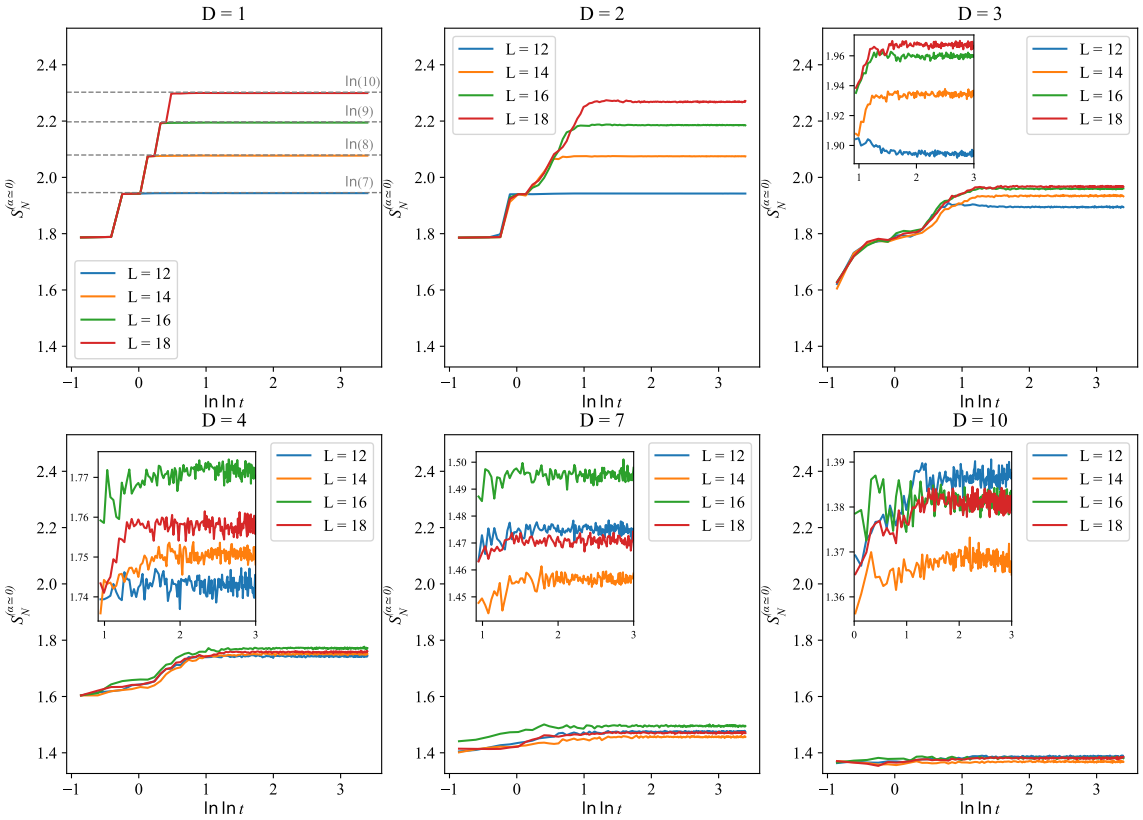

Figure 5.5: Time evolution of the Hartley entropy for a non-interacting system at various disorder strengths D and system sizes $L = 12, 14, 16, 18$. Each panel corresponds to a fixed disorder value. For disorder strengths below the critical value $D_c = 2$, the Hartley entropy exhibits a volume-law behavior. The step-like structures observed in this regime indicate changes in entropy, attributed to a single particle crossing the cut. As the disorder strength increases ($D > D_c$), the growth of entropy becomes suppressed, and the curves saturate, indicating localization. It also demonstrates the absence of volume-law scaling.

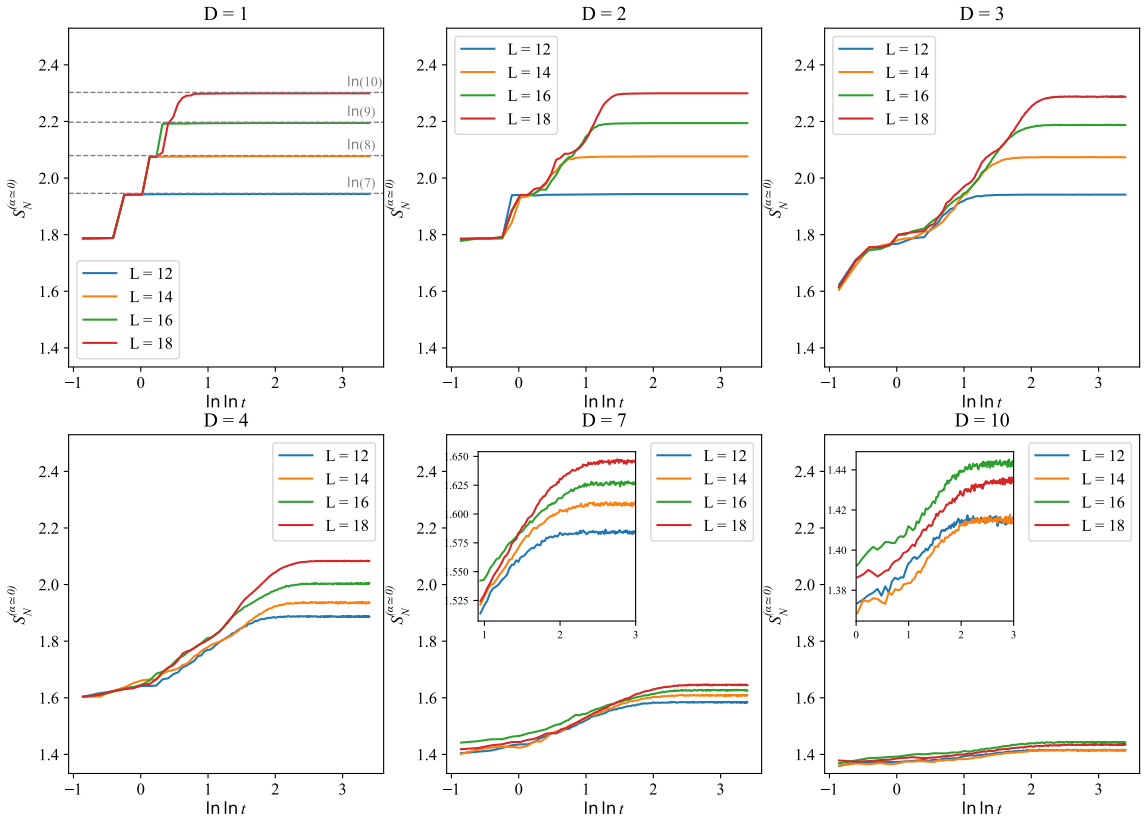

Figure 5.6: Time evolution of the Hartley number entropy $S_N^{(\alpha\simeq 0)}$ for the interacting system at various disorder strengths $D = 1, 2, 3, 4, 7, 10$, and system sizes $L = 12, 14, 16, 18$.

In Fig. 5.7(a), we observe that for disorder strengths $D < D_c$, the entropy saturates at the value where all particle-number configurations are explored ($S_N^{(\alpha\simeq 0)} = \ln 9$), indicating a thermal regime. The inset shows that in the presence of interactions, this growth follows a $\ln \ln t$ scaling for strong disorder ($D = 7, 8, 9, 10$), as mentioned above. By looking at the saturation value for the interacting case, we observe a form of volume-law scaling even at strong disorder (for $D = 10$ not a volume-law in the sense of linear growth with L, but at least a slow increase with L rather than a flat line). An interacting system at $D = 7$ for instance, still shows larger S, Fig. 5.4(c), and $S_N^{(\alpha\simeq 0)}$, Fig. 5.7(b), when $L = 18$ than when $L = 14$, indicating that larger systems have broader particle-number distributions. This contrasts with the non-interacting localized case.

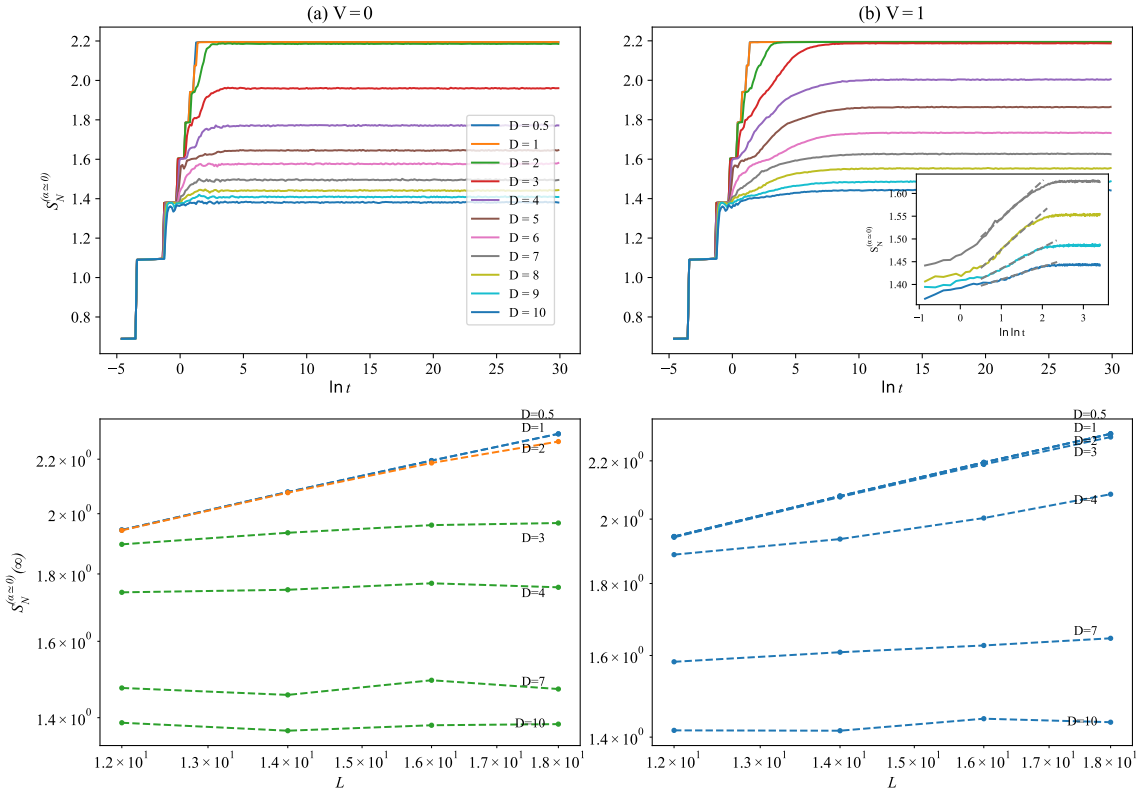

Figure 5.7: Comparison of the time evolution of the Hartley number entropy for $L = 16$ and saturation values of the Hartley number entropy as a function of L for various disorder strengths in (a) non-interacting and (b) interacting systems. The inset in the top right plot demonstrates a close-up picture of the Hartley number entropy scaled over $\ln \ln t$ for $D = 7, 8, 9, 10$.

Chapter 6

Conclusion

Our research was focused on quasiperiodic disordered systems instead of the randomly disordered case, and our results provided us with important information for the ongoing debate on the stability of the many-body localized phase in such systems. Our motivation to consider the Aubry–André model was to benefit from the absence of the avalanche mechanism to probe MBL stability since avalanches can spread and ultimately destroy localization. Quasiperiodic potentials such as the AA model do not feature the occurrence of large rare fluctuations which will eventually cause thermalizing bubbles, the primary driving force of avalanches. Thus, by introducing this model, we effectively remove this scenario; nevertheless, we still find that the interacting AA system shows no sign of true MBL dynamics. Although some work had suggested that large disorder strengths can make the MBL phase persist in quasiperiodic potentials, our results are more in line with those of Kiefer-Emmanouilidis and Sirker et al. [3], who had given very strong evidence that many-body localized phases do not exhibit true localization at long times.

In the case of the non-interacting AA model, we observed a clear difference between thermal and localized regimes. We confirmed Anderson localization transition at a critical disorder strength $D_c = 2J$. In the case of added interactions, our study revealed that although the entanglement entropy grows logarithmically, the number entropy exhibits unbounded growth, $S_N \sim \ln \ln t$, even in the presence of strong disorder. As for quenched disorder, this is again consistent with the relation $S_N \sim \ln S$ between the two entropies. Additionally, by examining the deviation time for the entanglement and number entropies, we made sure that both entropies evolve together

in time and there exists a correlated behavior; both of these entropies saturate at the time $t_d \sim e^D$ due to the finite Hilbert space. This is consistent with the hypothesis that an MBL regime in finite systems might eventually thermalize if given sufficient time. Our findings add to previous findings by extending them to the scenario of quasiperiodic MBL, demonstrating that the lack of true randomness does not change the intrinsic behavior of the MBL phase. Even more interestingly, the scaling behavior we observed for the prefactors μ and ν Fig. 5.2 aligns remarkably well with previous results [28], despite the fact that our model uses the Aubry-André potential instead of the random potential. This scaling relation $\mu, \nu \sim D^{-\alpha}$ emerges in both cases, with an almost identical exponent. We found $\alpha \simeq 3.06$ for $L = 16$ in our system, while Ref. [28] reported $\alpha \simeq 3.0$ for $L = 14$ for the random potential case.

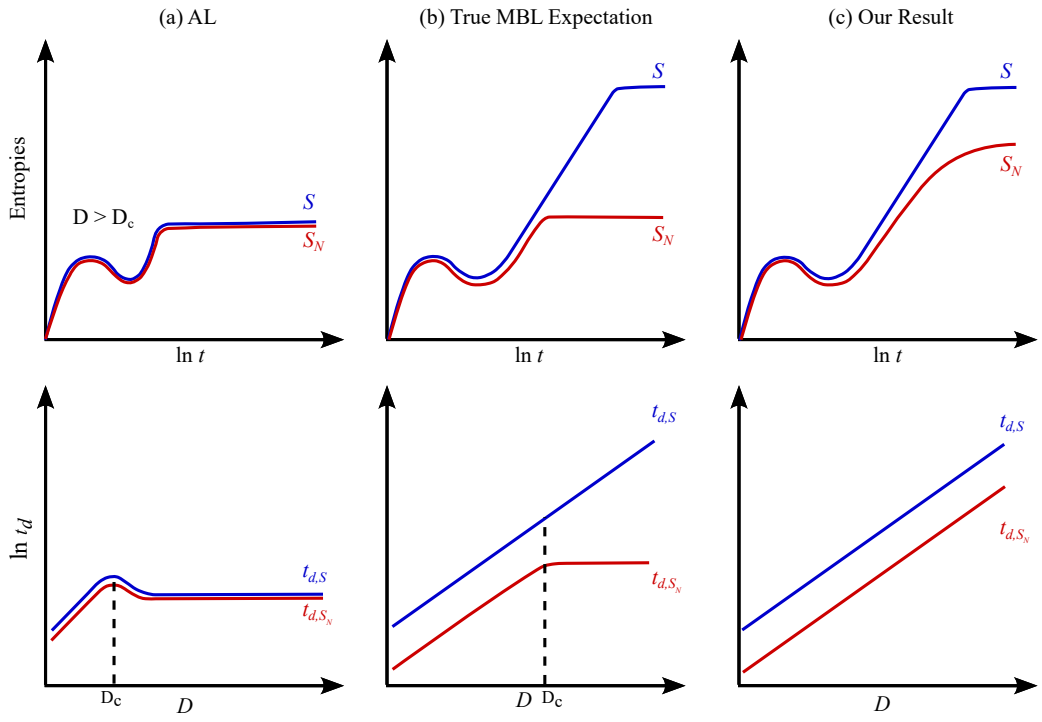

Figure 6.1: Comparison of entropy dynamics and saturation times across different localization scenarios for finite-size systems. The top row shows schematic behavior of entanglement and number entropies S_N over $\ln t$; the bottom row shows the corresponding saturation times over disorder strength D.

We also examined the Rényi number entropy for $\alpha \to 0$. In the system without interaction, for the ergodic phase where $D < D_c$, the Hartley number entropy grows with system size and when fully thermalized, it reaches all particle configurations with non-zero probability. In the system with interactions, we observed that a volume-law scaling remains even for $D > D_c$ with $D_c = 2$ being the critical disorder value for AL. Only at very large disorder strength $D = 10$, we begin to see that the behavior of the Hartley number entropy starts deviating from volume-law. However, even for this strong disorder ($D = 10$), the entropy did not saturate immediately and exhibits a logarithmic growth in time, similar to the standard number entropy, rather than a plateau. This finding, along with the above-mentioned ones, indicates that even at large disorder $D = 10$, the system does not exhibit a true many-body localized regime.

Bibliography

[1] P. W. Anderson. Absence of diffusion in certain random lattices. *Phys. Rev.*, 109:1492–1505, Mar 1958.

[2] D. M. Basko, I. L. Aleiner, and B. L. Altshuler. Metal-insulator transition in a weakly interacting many-electron system with localized single-particle states. *Ann. Phys.*, 2006.

[3] M. Kiefer-Emmanouilidis, R. Unanyan, M. Fleischhauer, and J. Sirker. Evidence for unbounded growth of the number entropy in many-body localized phases. *Phys. Rev. Lett.*, 124:243601, 2020.

[4] J. Suntajs, J. Bonca, T. Prosen, and L. Vidmar. Quantum chaos challenges many-body localization. *Phys. Rev. E*, 102:062144, 2020.

[5] Alan Morningstar, Luis Colmenarez, Vedika Khemani, David J. Luitz, and David A. Huse. Avalanches and many-body resonances in many-body localized systems. *Physical Review B*, 105:174205, 2022.

[6] M. Schreiber, S. S. Hodgman, P. Bordia, H. P. Lüschen, M. H. Fischer, R. Vosk, E. Altman, U. Schneider, and I. Bloch. Observation of many-body localization of interacting fermions in a quasi-random optical lattice. *Science*, 349:842, 2015.

[7] Vedika Khemani, David N Sheng, and David A Huse. Two universality classes for the many-body localization transition. *Phys. Rev. Lett.*, 119(7):075702, 2017.

[8] M. Rigol, V. Dunjko, and M. Olshanii. Thermalization and its mechanism for generic isolated quantum systems. *Nature*, 452:854–858, 2008.

[9] J. M. Deutsch. *Phys. Rev. A*, 43:2046, 1991.

[10] F. H. L. Essler and M. Fagotti. Quench dynamics and relaxation in isolated integrable quantum spin chains. *Journal of Statistical Mechanics: Theory and Experiment*, 2016(6):064002, 2016.

[11] J. E. Moore. A perspective on quantum integrability in many-body-localized and yang-baxter systems. *Philosophical Transactions of the Royal Society A: Mathematical, Physical and Engineering Sciences*, 375(2108):20160429, 2017.

[12] Rahul Nandkishore and David A. Huse. Many-body localization and thermalization in quantum statistical mechanics. *Annual Review of Condensed Matter Physics*, 6(1):15–38, 2015.

[13] Adam M. Kaufman, M. Eric Tai, Alexander Lukin, Matthew Rispoli, Robert Schittko, Philipp M. Preiss, and Markus Greiner. Quantum thermalization through entanglement in an isolated many-body system. *Science*, 353(6301):794–800, 2016.

[14] J. von Neumann. *Z. Phys.*, 57:30, 1929.

[15] P. Mazur. Non-ergodicity of phase functions in certain systems. *Physica*, 43:533, 1969.

[16] T. Prosen. Open xxz spin chain: Nonequilibrium steady state and a strict bound on ballistic transport. *Phys. Rev. Lett.*, 106:217206, May 2011.

[17] D. Faiez and D. Šafránek. How much entanglement can be created in a closed system. *Physical Review B*, 101(6):060401, 2020.

[18] U. Schollwöck. The density-matrix renormalization group in the age of matrix product states. *Ann. Phys.*, 326:96, 2011.

[19] V. Alba and P. Calabrese. Entanglement dynamics after quantum quenches in generic integrable systems. *SciPost Physics*, 4(3):017, 2018.

[20] M. Fagotti and F. H. L. Essler. Reduced density matrix after a quantum quench. *Phys. Rev. B*, 87:245107, 2013.

[21] Ingo Peschel and Viktor Eisler. Reduced density matrices and entanglement entropy in free lattice models. *J. Phys. A*, 42(50):504003, 2009.

[22] Jens H. Bardarson, Frank Pollmann, and Joel E. Moore. Unbounded growth of entanglement in models of many-body localization. *Phys. Rev. Lett.*, 109:017202, Jul 2012.

[23] Marcos Rigol. Breakdown of thermalization in finite one-dimensional systems. *Phys. Rev. Lett.*, 103:100403, Sep 2009.

[24] Alexander Lukin, Matthew Rispoli, Robert Schittko, M. Eric Tai, Adam M. Kaufman, Soonwon Choi, Vedika Khemani, Julian Leonard, and Markus Greiner. Probing entanglement in a many-body-localized system. *Science*, 364:256, 2019.

[25] M. Greiner, O. Mandel, T. Esslinger, T. W. Hänsch, and I. Bloch. Quantum phase transition from a superfluid to a mott insulator in a gas of ultracold atoms. *Nature*, 415:39, 2002.

[26] B. Paredes *et al. Nature*, 429:277, 2004.

[27] T. Bridges, A. Elben, P. Jurcevic, B. Vermersch, C. Maier, B. P. Lanyon, P. Zoller, R. Blatt, and C. F. Roos. Probing rényi entanglement entropy via randomized measurements. *Science*, 364:260, 2019.

[28] Maximilian Kiefer-Emmanouilidis, Razmik Unanyan, Michael Fleischhauer, and Jesko Sirker. Unlimited growth of particle fluctuations in many-body localized phases. *Annals of Physics*, page 168481, 2021.

[29] E. Abrahams, P. W. Anderson, D. C. Licciardello, and T. V. Ramakrishnan. Scaling theory of localization: Absence of quantum diffusion in two dimensions. *Phys. Rev. Lett.*, 42:673–676, Mar 1979.

[30] Katsuhisa Slevin and Tomi Ohtsuki. Critical exponent for the anderson transition in the three-dimensional orthogonal universality class. *New Journal of Physics*, 16:015012, 2014.

[31] B Kramer and A MacKinnon. Localization: theory and experiment. *Rep. Prog. Phys.*, 56(12):1469, 1993.

[32] Yang Zhao, Dingyi Feng, Yongbo Hu, Shutong Guo, and Jesko Sirker. Entanglement dynamics in the three-dimensional anderson model. *Phys. Rev. B*, 102:195132, Nov 2020.

[33] M. Kiefer-Emmanouilidis, R. Unanyan, J. Sirker, and M. Fleischhauer. Bounds on the entanglement entropy by the number entropy in non-interacting fermionic systems. *SciPost Phys.*, 8:083, 2020.

[34] Vadim Oganesyan and David A. Huse. Localization of interacting fermions at high temperature. *Phys. Rev. B*, 75:155111, Apr 2007.

[35] B. Kramer, G. Bergmann, and Y. Bruynseraede, editors. *Localization, Interaction, and Transport Phenomena*, Braunschweig, Fed. Rep. of Germany, August 23–28, 1984 1985.

[36] D. A. Evensky, R. T. Scalettar, and P. G. Wolynes. Localization and dephasing effects in a time-dependent anderson hamiltonian. *The Journal of Physical Chemistry*, 94(3):1149, 1990.

[37] D. E. Logan and P. G. Wolynes. Dephasing and anderson localization in topologically disordered systems. *Physical Review B*, 36:4135, 1987.

[38] Maximilian Kiefer-Emmanouilidis. *Particle Delocalization in Many-Body Localized Phases*. Phd thesis, Technische Universität Kaiserslautern, 2022.

[39] David J Luitz, Nicolas Laflorencie, and Fabien Alet. Many-body localization edge in the random-field heisenberg chain. *Phys. Rev. B*, 91:081103, 2015.

[40] D. Sels. Markovian baths and quantum avalanches. 2021.

[41] D. Sels and A. Polkovnikov. Dynamical obstruction to localization in a disordered spin chain. *arXiv: 2009.04501*, 2020.

[42] B. Bauer and C. Nayak. Area laws in a many-body localized state and its implications for topological order. *Journal of Statistical Mechanics: Theory and Experiment*, 2013(09):P09005, 2013.

[43] Dmitry A. Abanin, Ehud Altman, Immanuel Bloch, and Maksym Serbyn. Colloquium: Many-body localization, thermalization, and entanglement. *Rev. Mod. Phys.*, 91:021001, May 2019.

[44] Maksym Serbyn, Z. Papić, and Dmitry A. Abanin. Universal slow growth of entanglement in interacting strongly disordered systems. *Phys. Rev. Lett.*, 110:260601, Jun 2013.

[45] A. Pal and D. A. Huse. Many-body localization phase transition. *Phys. Rev. B*, 82:174411, Nov 2010.

[46] Maksym Serbyn and Dmitry A. Abanin. Loschmidt echo in many-body localized phases. *Physical Review B*, 96:014202, 2017.

[47] Kosuke Yamamoto and Ryusuke Hamazaki. Localization properties in disordered quantum many-body dynamics under continuous measurement. *Physical Review B*, 107:L220201, 2023.

[48] Marko Žnidarič, Tomasz Prosen, and Peter Prelovšek. Many-body localization in the heisenberg xxz magnet in a random field. *Phys. Rev. B*, 77:064426, Feb 2008.

[49] David A. Huse, Rahul Nandkishore, and Vadim Oganesyan. Phenomenology of fully many-body-localized systems. *Phys. Rev. B*, 90:174202, Nov 2014.

[50] Alexander Lukin, Matthew Rispoli, Robert Schittko, M. Eric Tai, Adam M. Kaufman, Soonwon Choi, Vedika Khemani, Julian Léonard, and Markus Greiner. Probing entanglement in a many-body–localized system. *Science*, 364(6437):256–260, 2019.

[51] Yi-Ting Tu, DinhDuy Vu, and S. Das Sarma. Avalanche stability transition in interacting quasiperiodic systems. *Phys. Rev. B*, 107:014203, Jan 2023.

[52] Svetlana Ya. Jitomirskaya. Metal-insulator transition for the almost mathieu operator. *Annals of Mathematics*, 150(3):1159–1175, 1999.

[53] M. Suzuki. Generalized trotter's formula and systematic approximants of exponential operators and inner derivations with applications to many-body problems. *Commun. Math. Phys.*, 51:183, 1976.

[54] H. F. Trotter. On the product of semi-groups of operators. *Proc. Amer. Math. Soc.*, 10:545, 1959.

[55] Maximilian Kiefer-Emmanouilidis, Razmik Unanyan, Michael Fleischhauer, and Jesko Sirker. Slow delocalization of particles in many-body localized phases. *Phys. Rev. B*, 103:024203, Jan 2021.